Chem Soc Rev

Heteroatom doped graphene materials: syntheses, properties and applications

Journal:	*Chemical Society Reviews*
Manuscript ID:	CS-REV-04-2014-000141.R1
Article Type:	Review Article
Date Submitted by the Author:	29-Apr-2014
Complete List of Authors:	wang, xuewan; NTU, Sun, Gengzhi; Nanyang Technological University, Routh, Parimal; Nanyang Technological University, Kim, Donghwan (Richie); Nanyang Technological University, School of Chemical and Biomedical Engineering Huang, Wei; Nanjing University of Technology, Institute of Advanced Materials Chen, Peng; Nanyang Technological University, School of Chemical & Biomedical Engineering

Heteroatom doped graphene materials: syntheses, properties and applications

Xuewan Wang[a], Gengzhi Sun[a], Parimal Routh[a], Dong-Hwan Kim[a], and Wei Huang[b], Peng Chen[a]*

[a]School of Chemical and Biomedical Engineering, Nanyang Technological University, 70 Nanyang Drive, 637457, Singapore

[b]Singapore-Jiangsu Joint Research Center for Organic/Bio-Electronics and Information Displays & Institute of Advanced Materials (IAM), Nanjing University Technology, 30 South Puzhu Road, Nanjing, 211816, China

*correspondence: ChenPeng@ntu.edu.sg

Abstract

Heteroatom doping can endow graphene with various new or improved electromagnetic, physicochemical, optical, and structural properties. This greatly extends the arsenal of graphene materials and their potentials for a spectrum of applications. Covering the latest developments, we comprehensively and critically discuss the syntheses, properties and emerging applications of the growing family of heteroatom doped graphene materials. Advantages, disadvantages, and preferential doping features of current synthesis approaches are compared, aiming to provide clues for developing new and controllable synthetic routes. We emphasize the distinct properties resulting from various dopants, different doping levels and configurations, and synergistic effects from co-dopants, hoping to assist a better understanding of doped graphene materials. The mechanisms underlying their advantageous uses for energy storage, energy conversion, sensing, and gas storage are highlighted, aiming to stimulate more exciting applications.

1 Introduction

In the past decade, we have witnessed the explosion and great success in graphene research since the first isolation of this "wonder material". Graphene has been changing the landscape of many fields in science and technology including particularly condensed matter physics, [1, 2] electronics,[3,

[4] energy storage and conversion,[5-7] and biomedical research.[8-10] Tremendous efforts are still ongoing to uncover the full potential of graphene and its derivatives.

The fantastic properties of pristine graphene (single-atom-thick layer of sp^2 bonded carbon atoms tightly packed into a 2D honeycomb lattice) are now largely understood and well-recognized through the extensive research in the past years.[11-13] Although the lack of intrinsic bandgap and catalytic abilities seems to greatly limit practical applications of pristine graphene, the legend of this 2D material is doomed to continue owing to its structural transformability and highly tunable properties. As demonstrated more recently, new properties and application opportunities arise when graphene transforms from its native 2D structure to 0D (graphene quantum dots),[14-17] 1D (grahene nanoribbon)[18, 19] or 3D (graphene foam) structure.[20-22] In addition, the physicochemical and electronic properties of graphene can be drastically altered by molecular and atomic doping.

Tailoring graphene properties by interacting molecules which either donate or withdraw free electrons have been demonstrated in many studies and discussed in the recent review articles.[23-25] Herein, we focus the discussion on doping of graphene with various heteroatoms (oxygen, boron, nitrogen, phosphor, sulfur, etc.), i.e., the graphitic carbon atoms are substituted or covalently bonded by foreign atoms. Although several review articles focusing on specific dopants or particular applications have been published,[26-29] a more comprehensive and comparative review on this important and quickly evolving topic is necessary. In this article, the synthesis methods, properties and applications of graphene materials doped with various heteroatoms are extensively reviewed. We aim to cover the latest developments, underscore physical mechanisms, highlight unique application-specific advantages conferred by doping, and provide insightful comparison between doped and pristine graphene, different synthesis routes, different dopant atoms, and different doping configurations.

2 Synthesis Methods

A large variety of methods have already been developed for synthesis of graphene materials, from which various doping strategies could be derived. The current methods for heteroatom doping can be categorized into in-situ approaches and post-treatment approaches. In-situ approaches, which

achieve graphene synthesis and heteroatom doping simultaneously, include chemical vapor deposition (CVD), ball milling, and bottom-up synthesis. Post-treatment methods include wet chemical methods, thermal annealing of graphene oxides (GO) with heteroatom precursors, plasma and arc-discharge approaches. In this section, these methods are discussed and compared in details (Table 1).

Table 1 Summary of graphene doping techniques

Methods	Precursors	Doping	Advantages and limitations	Ref.
CVD	H_3BO_3+polystyrene	4.3 at% B	Simultaneous growth and doping of large graphene sheet; controllable doping; complex process and high operating temperature;sometimes hazardous precursors and waste gases;high cost and low yield.	31
	Phenylboronic acid	1.5 at% B		36
	CH_4+H_3NBH_3	10-90 at% BN		33
	CH4+NH_3	8.9 at% N		42
	Sulfur in hexane	< 0.6 at% S		44
	Iodine+camphor	3.1 at% I		46
	Pyrimidine+thiophene	⩽5.7 N, 2.0 S at%		45
Ball milling	Pristine graphite (PG)+N_2	14.8 wt% N	Simple and scalable process;doping only at edges; difficult to control the doping process.	49
	PG+ sulfur powder	4.94 at% S		53
	PG+ Cl_2/Br_2	5.85Cl/2.78 Br at%		51
Bottom-up synthesis	CCl_4+K+BBr_3	2.56 at% B	Scalable solution-based reaction at mild condition;unavoidable high oxygen content.	54
	Li_3N+CCl_4	4.5-16.4 at% N		55
	pentachloropyridine+K	3.0 at% N		56
Thermal annealing	GO+BCl_3	0.88 at% B	Wide choices of dopant precursors (gases, liquids, or solids);controllable doping;high temperature required, but helpful to recover sp^2carbon network.	59
	GO+NH_3	8 at% N		63
	GO+melamine/PANI/PPy	2-18 at% N		70, 71
	GO+ionic liquid	22.1 N/1.16 P at%		75,76
	GO+H_2S	1.2-1.7 at% S		77
	GO+DDS+DDSe	0.19 S, 0.05 Se at%		80
	Graphite oxide+Cl_2/Br_2	5.9 Cl/ 9.93 Br at%		84
Wet chemical method	GO+hydrazine	4.5 at% N	Amenable to low-cost, low-temperature, solution-based mass production;easily achieve doping and decoration (e.g.,with various nanoparticles) simultaneously;conveniently form 3D gel structure.	86
	GO+urea	10.13 at% N		91
	GO+NH_4SCN	18.4 N, 12.3S at%		95
	GO+HF/HI	1.38 F/ 4.33 I wt%		96
	PG+Cl_2/Br_2	21 Cl/ 4 Br at%		99
Plasma	GO+N_2	2.51at% N	Short reaction time and low power consumption;low yield.	108
	CVD graphene+Cl_2	45.3 at% Cl		112
Photo-chemistry	CVD graphene+Cl_2, xenon lamp irradiation	8 at% Cl	Short reaction time and low power consumption; low yield.	113
Arc-discharge	PG+NH_3	1 at% N	Mass-production; high voltage or current required; low doping level; mainly multilayer graphene.	114
	PG+B/B_2H_6	3.1 at% B		115
	PG+graphite fluoride	10 wt%		116

2.1 In situ doping

2.1.1 Chemical vapor deposition (CVD)

Many CVD methods have been developed to synthesize large-sized, continuous, defect-free, single- or few-layered graphene film. The catalytic growth mechanism makes it convenient route to dope heteroatoms during the formation of graphene film, particularly, to incorporate heteroatoms directly into the graphitic carbon lattices. As illustrated in Fig. 1a[30], doping can occur by introducing solid, liquid, or gas precursors containing desired foreign atoms into the growth furnace together with carbon sources. In some cases, carbon and foreign atom(s) share the same precursor. Co-doping of multiple species may also be achieved, aiming to create synergy between the co-dopants.

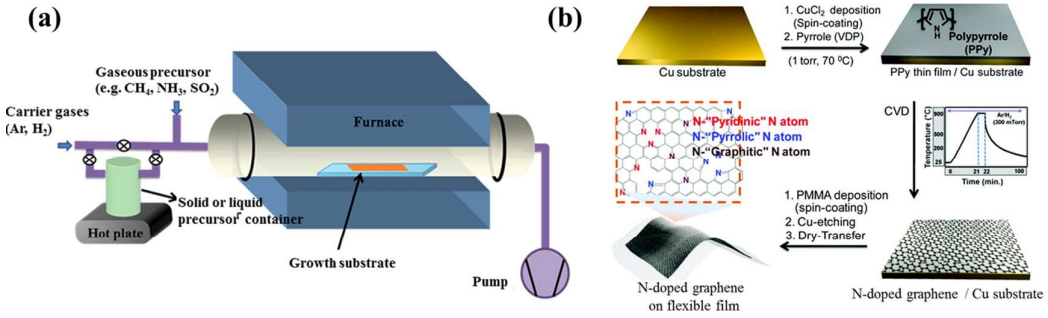

Fig. 1 (a) Experimental setup commonly used for CVD grahpene doping. Adapted with permission from ref. 30. Copyright (2013) American Chemical Society. (b) N-doped graphene derived from polypyrrole. Adapted with permission from ref. 39. Copyright (2012) American Chemical Society.

Because boron (B) and nitrogen (N) have similar size and valence electron number as carbon (C), it is relatively easier to incorporate them into graphene. For example, B-doped graphene with a doping level of 4.3 at% (atomic percentage) was grown on copper (Cu) foil at 1000 °C under the protection of H_2/Ar atmosphere, using boric acid and polystyrene as B and C sources, respectively.[31] These solid-phase feedstocks are sublimated upstream and transported by the carrier gases to the growth substrate (Fig. 1a). B-doping was also realized using ethanol as the carbon source and boron powder as B-precursor.[32] There are two bonding configurations of B atoms observed in CVD graphene lattice: "boron silane" boron (BC_4) and graphitic boron (BC_3). In contrast to more commonly occurred BC_3 bonding (B replacing C in the hexagonal carbon

lattice), BC_4 configuration is resulted due to excess defects or edge sites. Dual B, N doped graphene was reported by Ajayan's group, using methane and ammonia borane (NH_3-BH_3) as the carbon and B,N sources, respectively.[33] The doping level can be tuned by adjusting the reaction parameters. At high doping levels, the resultant large-area B,N co-doped graphene contains B-N hybridized domains (with B/N ratio ~1) as evidenced by X-ray photoelectron spectroscopy (XPS) analyses. Incorporation of small BN domains (B/N ratio, 0.3~0.5) was also reported by Bepete *et al.*, employing boric acid powder and N_2 the precursors.[34] Using nickel foam as the growth template, B, N, or (B,N)-doped 3D graphene was also reported, which, compared with the 2D counterparts, offers large active surface area.[35]

In comparison with the use of multi-precursors, single precursor containing both C and alien atom is believed to be more convenient and controllable. For instance, homogeneous B-doping on graphene monolayer was produced using phenylboronic acid as the sole precursor, without significantly compromising the transmittance and conductivity of the graphene film.[36] Pyridinic and pyrrolic-N doped graphene was synthesized using acetonitrile as the only precursor[37] while pyridinic-N doped graphene was CVD-grown using pyridine as the sole source.[38]

Heteroatom containing polymers (sometimes embedded in polymeric carrier matrix) can be directly vapor-deposited or spin-coated atop metal catalyst for graphene growth and in situ doping. Such processes are safer without the use of high-temperature gases and can achieve patterned doping. In the work of Kwon *et al.*, pyrrole monomers vapored on Cu substrate were polymerized by the presence of Cu^{2+} ions, followed by CVD growth (Fig. 1b).[39] The obtained N-doped few-layered graphene contains 3.14 at% N with dominating pyrrolic N likely inherited from the ploypyrrole precursor. Sun *et al.* directly spin-coated the mixture of N-rich melamine and PMMA on Cu substrate for growth of N-doped graphene at 1000 °C under atmospheric pressure, reaching a doping level of 2-3.5 at%.[40] It is known that melamine can evolve into two-dimensional graphene-like graphitic carbon nitride (g-C_3N_4).[41] Although the configuration of N-doping is mainly graphitic, the mobility of the obtained N-graphene is poor (<10 $cm^2 V^{-1} s^{-1}$).[40]

Gaseous precursor is most commonly used, for which the doping level can be readily controlled by the flow rates (thus the percentage ratio between the gaseous reactants). Wei *et al.* firstly reported the experimental synthesis of N-doped graphene with CH_4 and NH_3 as the C and N sources.[42] Growth temperature and the ratio between CH_4 and NH_3 exert great influence on the

bonding structure of doped nitrogen. The few-layered N-graphene synthesized at 800 °C enjoys a high N level of 8.9 at%, among which graphitic N are the dominant species (comparing to the co-existing pyridinic and pyrrolic N)[42] whereas N-doped graphene synthesized at 1000 °C exhibits dominating pyridinic N and a small fraction of pyrrolic N.[43]

Fluorine gas (F_2) and F-containing compounds are toxic and too reactive at high temperature. Therefore, to our best knowledge, there is still no report on the synthesis of F-doped graphene using CVD method. And it is energetically unfavorable to incorporate large-sized atoms (e.g., silicon - Si, phosphorus - P, sulfur - S, chlorine - Cl, iodine - I) into graphene. Gao *et al.* demonstrated the CVD growth of S-doped graphene on Cu substrate using sulfur powder dissolved in hexane as the precursor.[44] But the S-doping level is extremely low (< 0.6 at%), likely in the form of -C-S-C- and preferably at the defect sites due to lowered binding energy. Xu *et al.* synthesized N,S co-doped graphene at a relatively low temperature of 700 °C using pyrimidine (N, C source) and thiophene (S, C source) as the precursors.[45] N and S atoms in the co-doped graphene are uniformly distributed with doping level of 3.7 to 5.7 at% and 0.7 to 2.0 at%, respectively. Apart from the -C-S-C- bonding configuration, -C-SO_x-C- is also speculated to exist. I-doped graphene was also made using CVD method, in which iodine and camphor mixture was evaporated and pyrolyzed on a nickel substrate at 800 °C for 3 min.[46] All I atoms (3.1 at%) are doped *via* ionic bonding in aggregated forms (e.g., I_3^- and I_5^-).

2.1.2 Ball milling

CVD approaches, however, are of high-cost, only suitable for synthesizing thin-film graphene, and not amenable to mass-production. In comparison, ball milling is an effective way to massively produce graphene nanosheets at low-cost by delaminating graphite and cracking C-C bonds. It provides unique possibility for graphene doping. The freshly formed active carbon species (e.g. carboradicals, carbocations and carbanions) at the edges can readily react with the dopants *via* mechanochemistry. Such edge-selective functionalization process preserves the high crystallinity of graphene basal plane (thus electronic properties of graphene).[47, 48]

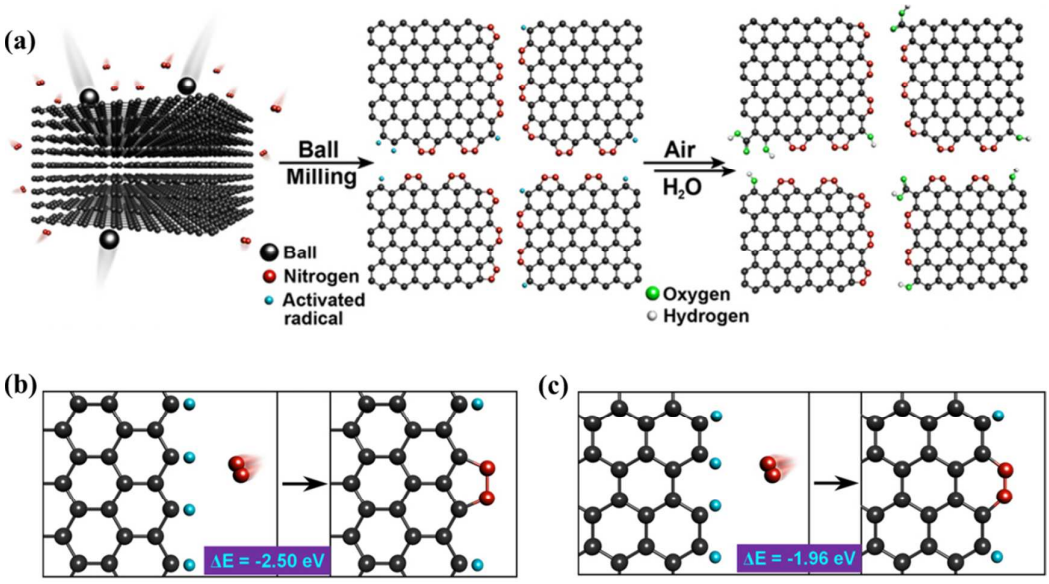

Fig. 2 (a) A schematic representation of physical cracking of graphite flake in a ball-mill crusher in the presence of nitrogen and subsequent exposure to air moisture to produce N-doped graphene nanoplates. (b and c) The formation of 5-membered pyrazole ring / 6-membered pyridazine ring after the reaction between the active zigzag-edge carbon atoms / armchair-edge carbon atoms and nitrogen. Adapted with permission from ref. 49. Copyright (2013) Nature Publishing Group.

By ball-milling graphite under N_2 atmosphere over 48 h, Jeon *et al.* successfully fixed uncleaved N_2 at the broken edges of graphene nanoplates with a high nitrogen content of 14.84 wt% (weight percentage) (Fig. 2a).[49] They proposed that aromatic 5-membered pyrazole and 6-membered pyridazine rings are energy-favorably formed at zigzag and armchair edges, respectively (Fig. 2b and c). It is more likely to form zigzag edges due to its larger density of states near the Fermi level than that of armchair edges.[50] However, the stability of 5N ring at zigzag edges is inferior to 6N ring at armchair edges. The entropy gain from grain size reduction and enthalpy increase from the edge functionalization facilitates dispersion of graphene nanoplates in various polar solvents (e.g. water, methanol, isopropyl alcohol, DMF and NMP).[51, 52] This is desirable for further solution-based processes.

Edge-sulfurized graphene nanoplatelets (SGnP) were also prepared by ball milling graphite in the presence of sulfur (S_8), with uniformly-distributed sulfur elements at a level of 4.94 at%.[53] Similarly, halogen atom doped grahpene nanoplates (ClGnP, BrGnP and IGnP) were synthesized in the presence of chlorine (Cl_2), bromine (Br_2) or iodine (I_2), respectively.[51] The decreasing

doping levels (Cl at 5.89, Br at 2.78, and I at 0.95 at%) correlate with the decreasing chemical reactivity and increasing size of these elements. Analogous to ball milling, N-doping of graphene was achieved while mechanically exfoliating graphene sheets by scotch-taping graphite in nitrogen ambient.[50] The freshly generated edges were immediately passivated by nitrogen. Because doping and defects were absent in the basal plane, a high mobility of 5000 cm^2 V^{-1} s^{-1} was measured.

2.1.3 Bottom-up synthesis

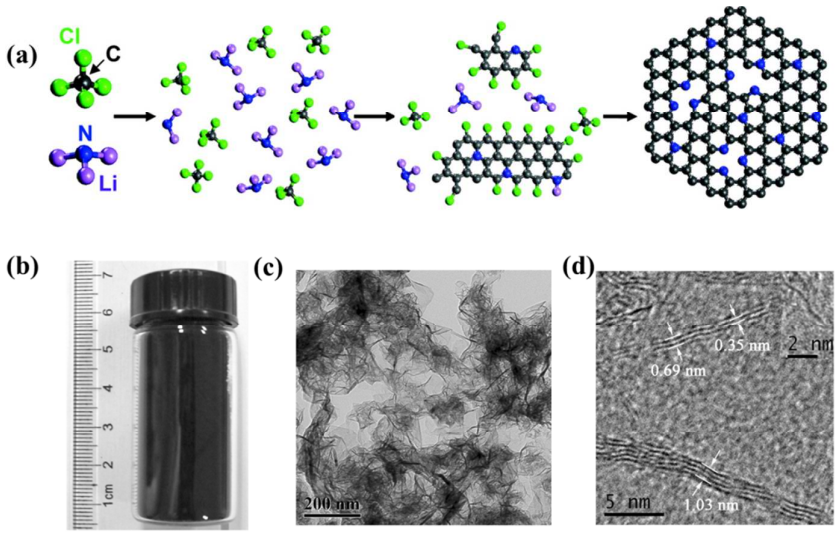

Fig. 3 (a) Proposed mechanism for solvothermal synthesis of N-doped graphene *via* the reaction of CCl_4 and Li_3N, where gray balls represent C atoms, blue for N, green for Cl, and purple for Li. (b) Vial containing prepared N-doped graphene sample. (c and d) TEM images of synthesized N-doped graphene samples. Adapted with permission from ref. 55. Copyright (2011) American Chemical Society.

Wurtz-type reductive coupling (WRC) reaction has been proposed as a bottom-up method for preparation of high-quality heteroatom-doped graphene. By reacting tetrachloromethane (CCl_4) with potassium (K) in the presence of boron tribromide (BBr_3) at a mild condition (210 °C, for 10 min), B-doped few-layer graphene was successfully synthesized with a doping level of 2.56 at% which could be tuned by adjusting the amount of B precursor.[54] Similarly, gram-scale of N-doped graphene (4.5~16.4 at%) was synthesized from lithium nitride (Li_3N) and CCl_4 at 120 ^oC for 12 h or cyanuric chloride mixed with Li_3N and CCl_4 at 350 ^oC for 6 h.[55] Graphitic N is prominent in the

former reaction while pyridinic and pyrrolic N are prevalent in the latter. Pyridinic N- and graphitic N-doped graphene was obtained by reacting pentachloropyridine with potassium at 160 °C.[56] Three reaction steps have been proposed for the formation of B/N-doped graphene (Fig. 3): (1) striping off halogens from halides; (2) coupling and assembly of freshly formed -C=C- and –C=B/N- into two-dimension hexagonal carbon cluster; (3) growth of B/N-doped graphene from these clusters.[54] Doping level can be readily controlled by the amount of heteroatom precursor for WRC reaction. In comparison with CVD growth, it does not require transition metal catalysts, but high oxygen content will be unavoidably introduced.[57] Peng *et al.* developed a different strategy to synthesize N-doped graphene-like sheets by annealing the mixture of PANI and melamine with the addition of Fe^{3+} ions at 900 °C.[58] Fe is believed to catalyze the formation of sheet structure.

2.2 Post-synthesis treatment

2.2.1 Thermal annealing

Graphene oxides (GO) prepared by chemical exfoliation approaches can be regarded as O-doped graphene materials. The abundant oxygen functional groups and defects on GO can act as reactive sites for doping of other heteroatoms. Thermal annealing of GO or reduced GO (rGO) at high temperature is effective to recover the sp^2 carbon network and simultaneously achieve heteroatom doping with the presence of appropriate precursors. For instance, annealing rGO in BCl_3 and Ar atmosphere at 800 °C for 2h or in NH_3 and Ar atmosphere at 600 °C, B-doped (0.88 at%) or N-doped (3.06 at%) graphene was obtained.[59] Under such low annealing temperature, only pyridinic N and pyrrolic N are formed. Different from the samples prepared by CVD, B atoms are doped in the forms of BC_3 and BC_2O, which might be due to the high oxygen content on rGO. Higher temperature is favorable for the formation of B-C bonding rather than B-O bonding.[60] N-doping is more commonly realized by annealing GO under high-purity ammonia gas (NH_3) which is not only a nitrogen source but also even a more effective reducing agent than H_2.[61]

It is unambiguous that temperature is a key factor to determine the N-doping efficiency and bonding configuration. Annealing GO in low-pressure NH_3/Ar atmosphere at different temperatures (from room temperature to 1100 °C), Li *et al.* found that N doping starts to occur at 300 °C and reaches the highest doping level of ~5 at% at 500 °C.[61] It is proposed that 500 ~ 600 °C is optimal for the overall stability of all N species (amino, pyrrolic, pyridinic and possibly

graphitic N).[62] Using such temperature, an even higher N-doping level of ~8 at% was reported.[63, 64] At lower temperature (300~500 °C), N bonding configurations include amino, amide, and pyrrolic N. The amino groups dominate as amino free radicals from ammonia react with the oxygenated groups on GO. In contrast, pyridinic and pyrrolic N are dominant at a temperature >800 °C.[65-68] At a further elevated temperature, some of pyridinic and pyrrolic N may be burnt by oxygen released from GO, leading to decrease of N content.[66] It was reported that annealing at 1100 °C for a long time promotes formation of graphitic N in the carbon lattice.[67] These observations are consistent with the thermal stability of different N bonding configurations: graphitic N > pyridinic N > pyrrolic N. Dai *et al.* demonstrated B,N co-doped graphene by simply thermal annealing GO in the presence of boric acid and NH_3 at 1000 °C.[69] They also suggested that increase of annealing time facilitates the formation BN clusters.

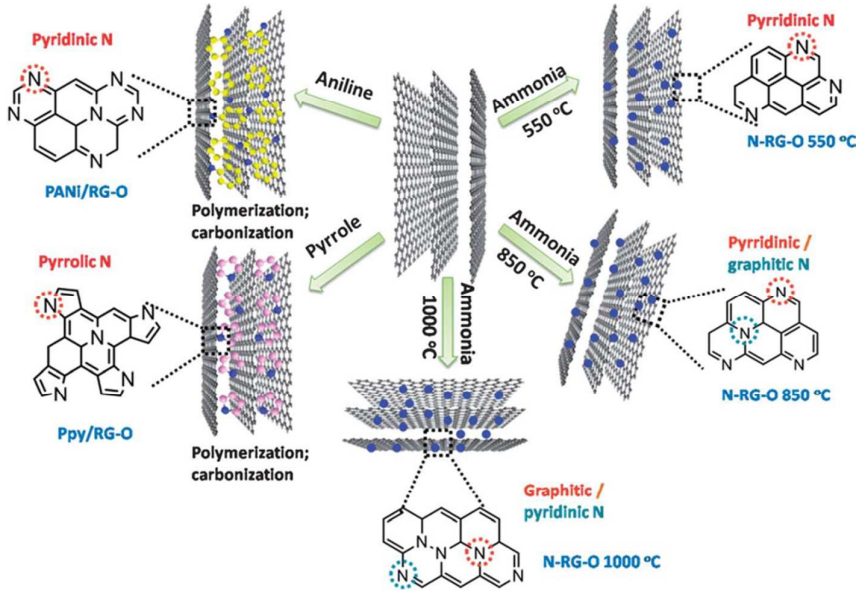

Fig. 4 N-doping configuration depends on the precursor and temperature. Adapted with permission from ref. 70. Copyright (2012) Royal Society of Chemistry.

In addition to annealing temperature, doping efficiency and configuration also critically depend on the chosen precursor(s) (Fig. 4).[70] In addition to NH_3, melamine,[71] polyaniline (PANI),[70, 72] polypyrrole (Ppy),[70] cyanamide[73] and dicyandiamide[74] have also been employed. Using these precursors, N-doping level ranges from 2 to 18 at%. Ionic liquids (IL), which contain N and/or P and whose surface tension and surface energy match well with that of graphene, can serve as excellent doping sources. Liu *et al.* annealed IL-electrolyzed graphene at a really low temperature

of 400 °C and obtained a high N/C ratio of 22.1%.[75] N bonding configuration is strongly dependent on the charge characteristics, viscosity, and other properties of the used ILs. For example, N-doped graphene synthesized using 1-butyl-3-methylimidazolium bromide ([Bmim]Br) shows the presence of pyrrolic N (major species) and graphitic N. In comparison, [Bmim][Ac] produced N-doped graphene shows dominant pyridinic N while [Bmim]PF_6 produced N-doping is equally contributed by pyridinic and pyrrolic forms. Also using [Bmim]PF_6, but annealed at 1000 °C, P-doped graphene nanosheets (3~4 layers) were obtained.[76] P-doping (1.16 at%) equally exist in two bonding configurations: P-C and P-O.

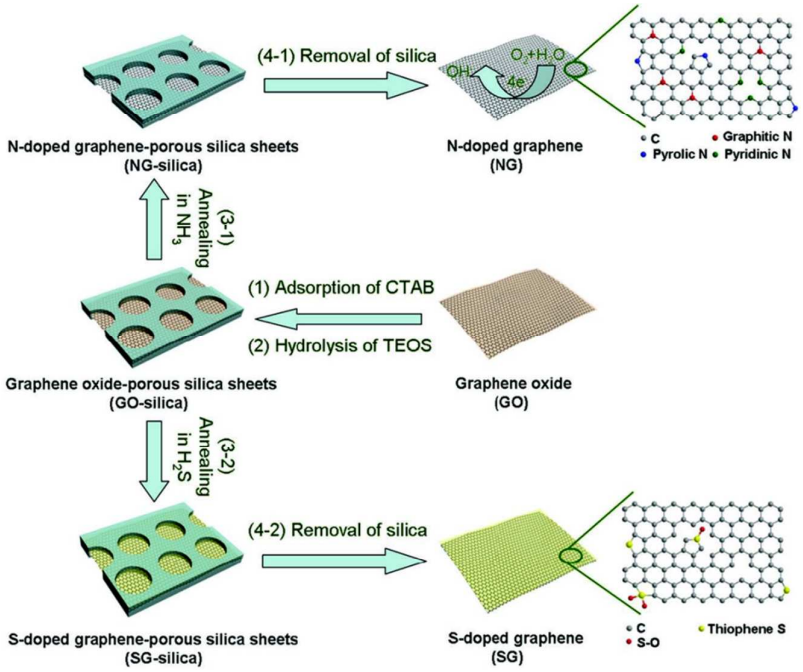

Fig. 5 N- or S-doping on porous silica confined GO sheets by thermal annealing. Adapted with permission from ref. 77. Copyright (2012) Wiley Publishing Group.

To avoid aggregation during the annealing process and ensure free gas transport, Yang *et al.* used porous silica to confine GO sheets for N- or S-doping (Fig. 5).[77] It was found that S-doping (1.2 - 1.7 at%) is less effective than N-doping and S-doping occurs at the defect sites forming thiophene-like structures. The properties of GO (the abundance and composition of oxygenated groups) and S-source chosen (H_2S, SO_2 or CS_2) exert great influences on doping.[78] Seredych *et al.* doped S into graphene by heating rGO in H_2S at 800 °C and 3 at% of S was introduced in thiophenic groups and aromatic rings.[79] The XPS analyses indicate that neutral S, -SH, -S_2-O- and

-SO- co-existed in the resultant materials. The solid precursors normally used for S/Se doping include dipheyldisulfide (DDS),[80] phenyl disulfide (PDS),[81] benzyl disulfide (BDS),[82, 83] and diphenyl diselenide (DDSe).[80, 82] Using BDS and melamine as the precursors, N,S co-doped graphene was produced with 2.0 at% of S and 4.5 at% of N.[83]

For halogen doping, Poh *et al.* successfully synthesized Cl-, Br- and I-doped graphene (with the doping level of 5.9, 9.93 and 2.31 at%, respectively) by thermal exfoliation / reduction of graphite oxide in halogen gas atmosphere.[84] Considering the poor thermal stability of halogen doped graphene, the doping process is conducted in a vacuum tight reactor with rapid temperature ramping / cooling rates. Similar to CVD processes, I-doping by this thermal process also relies on ionic bonding. The conductivity of Cl-graphene, Br-graphene and I-graphene increases in order. On the other hand, their thermal stability decreases in order in oxygen (but opposite in argon). Alternatively, Yao *et al.* prepared I-graphene by annealing GO and iodine in argon.[85] With the increase of temperature from 500 to 1100 °C, the content of I decreases from 1.21 to 0.83 wt%.

2.2.2 Wet chemical methods

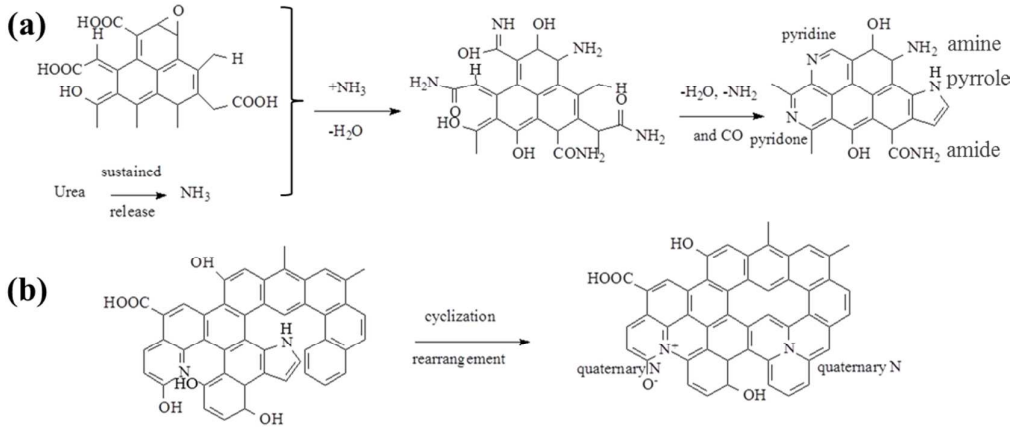

Fig. 6 Schematic illustration of (a) nitrogen insertion routes in GO (b) routes for the formation of a hypothetical structure of graphitic N in GO. Adapted with permission from ref. 91. Copyright (2012) Royal Society of Chemistry.

We have discussed a number of doping strategies above. But most of these methods suffer from the requirement of complex procedures and/or harsh conditions, low yield, or high cost. Therefore, efforts have been made for low-cost mass-production of doped graphene materials in solution phase. Because of its ampiphilic property, GO can be well-dispersed in water and various solvents

and the oxygen functional groups on its surface provide convenient chemical handles for reaction with heteroatom precursors. Hydrazine has been used for simultaneous GO reduction and N-doping in solution.[86, 87] Ruoff's group reported that, by hydrazine reduction, five member pyrazole rings with N_2 moiety form at the edges of GO sheet.[88] Ammonia solution (NH_4OH) is another widely adopted N precursor due to its high reactivity at relative low temperature (e.g. 80 °C).[89, 90] Urea,[91] hexamethylenetetramine,[92] dicyandiamide,[93] and hydroxylamine[94] can also serve as the precursors for N doping because their decomposition leads to gradual release of NH_3 during the hydrothermal process. Slow release of reactive NH_3 is desirable for high doping level. Taking advantage of this, Sun *et al.* synthesized N-graphene (10.13 at% doping) using urea.[91] They proposed that NH_3 continually reacts with the oxygen functional groups of GO (e.g. -COOH, -OH) for the initial formation of amide and amine intermediates, which then instantaneously reorganize by dehydration and decarbonylation to form more stable pyridine- and pyrrole-like structures (Fig. 6a). Graphitic N can form with increasing the reaction time resulting from cyclization rearrangement (Fig. 6b).

Su *et al.* used NH_4SCN, which decomposes into highly reactive species (NH_3, H_2S, CS_2) under hydrothermal condition, for N,S co-doping on GO.[95] Homogeneous doping of S (12.3 at%) and N (18.4 at%) is achieved. N exists in pyridinic (64%) and graphitic (36%) forms while S mainly dopes at defect sites and edges in the form of -C-S_n-C- (n=1 or 2, 55%), -C=S- (35%) and other moieties (e.g. -SO_n-, -SH). Garrido *et al.* modified GO with halogen atoms by hydrothermal approaches in HX solutions (X=F, Cl, Br or I), with doping level of 4.38 (F), 2.28 (Cl), 5.36 (Br), and 4.33 (I) wt%.[96]

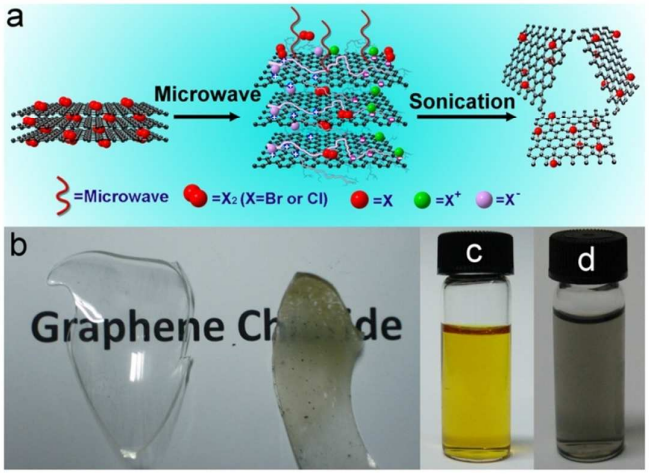

Fig. 7 (a) Synthesis of Cl- or Br-doped single-layer graphene sheets using microwave-spark method. (b) Photographs of the graphite chloride coated on the inside surface of the flask. (c and d) Photograph of Cl- and Br-doped graphene dispersion in DMF, respectively. Adapted with permission from ref. 99. Copyright (2012) Nature Publishing Group.

Halogen-doped graphene can also be obtained by liquid-phase-exfoliation (e.g., sonication) of graphite halide.[97, 98] But the doping level cannot be tuned using such methods, and it is usually challenging to make a large amount of halogenated graphite except fluorinated graphite. Recently, Zheng *et al.* developed an interesting microwave-spark method to synthesize Cl- and Br-doped graphite in the presence of liquid chlorine and bromine, which could then be easily exfoliated into single-layered Cl-/Br-doped graphene sheets *via* sonication (Fig. 7).[99] Under the luminous microwave-sparks, active graphite flakes generated by a short temperature shock can react with halogen precursors. Subsequent rapid temperature decrease quenches the reaction and prevents the thermal decomposition of the resultant materials. The obtained graphene sheets contain high percentages of covalently bonded Cl and Br (21 at% and 4 at%, respectively). Different from GO, the resulting doped-graphene is strongly hydrophobic and disperses well in organic solvents (Fig. 7).

Using wet chemical methods, heteroatoms have also been doped on 3D graphene gels which exhibit large surface area and macroporous structure.[94, 95, 100, 101] For example, Wu *et al.* employed ammonia boron trifluoride (NH_3BF_3) for co-doping of B and N.[101] Simultaneous reduction and self-assembly of GO sheets under the hydrothermal condition plus the subsequent freeze-drying process cause the formation of B,N-doped rGO aerogel. Solution-based doping processes also permit simultaneous decoration of various functional nanomaterials (e.g. metallic nanoparticles,[102] metal oxide nanoparticles[103-107]). The doped heteroatoms facilitate the nucleation and anchoring of these nanoparticles.

2.2.3 Other approaches

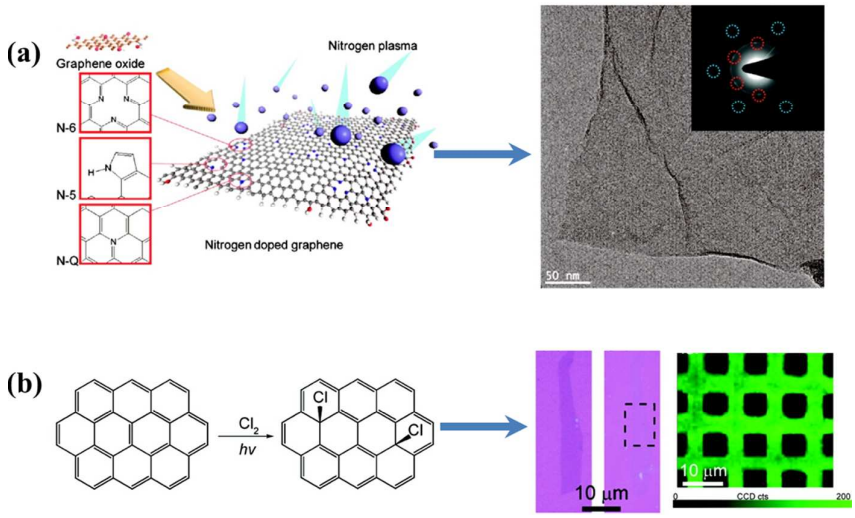

Fig. 8 (a) Schematic illustration of nitrogen plasma doping process with possible N configurations (left side); a high-resolution TEM image (right side) and selected area electron diffraction (inset) of the N-doped graphene indicated that the intrinsic layered structure and original honeycomb-like atomic structure were preserved during the plasma process. Adapted with permission from ref. 108. Copyright (2011) American Chemical Society. (b) Scheme of the photochemical chlorination process (left); optical images of a single-layer graphene sheet before and after photochemical chlorination, respectively (right, blue colour); D band mapping (λ_{ex} = 514.5 nm) of CVD-grown graphene film after a patterned photochlorination (right, green colour). Adapted with permission from ref. 113. Copyright (2011) American Chemical Society.

With short reaction time and low power consumption, plasma treatment is an effective method for heteroatom doping. Jeong *et al.* successfully achieved N doping in N_2 plasma (500 W in power, 14 Torr of N_2 gas) using H_2-plasma treated GO as the starting material (Fig. 8 a).[108] Large amount of defect sites produced from the H_2 plasma reduction process improves the effectiveness of N doping on the graphene basal plane. N-doping level and bonding configurations can be tuned by varying the aging time in N_2 plasma. The maximum N content of 2.51 at% was obtained after 3-min plasma treatment. During the plasma process, pyrrolic N which preferably forms at the defect sites continuously increases while graphitic N decreases and pyridinic N remains steady. NH_3 plasma is more reactive than N_2 plasma.[109, 110]

However, the level of N-doping attainable by plasma treatment is generally less comparing to

other doping methods. Plasma technique is particularly effective for halogen atom doping because halogen atoms are highly reactive. Wu *et al.* demonstrated plasma-assisted chlorine-doping on CVD graphene at a low power, without generation of much defects.[111] Cl coverage of 8.5 at% and conductance enhancement due to p-doping effect were observed. Tuning the plasma conditions (reaction time, dc bias, and vacuum level, *etc.*), Zhang *et al.* achieved extremely high Cl-doping of 45.3 at% (close to C_2Cl) on CVD graphene.[112] The C/Cl ratio and bonding states (C-Cl interaction through ionic bonding, covalent bonding, and defect creation) are sensitive to the dc bias applied. Li *et al.* developed a photochemical method for homogeneous and patternable Cl-doping on graphene (Fig. 8b).[113] Under the xenon lamp radiation (maximum power density of 1.4 W cm^{-2}), chlorine molecules split into highly reactive radicals which, in turn, covalently conjugate to the basal carbon atoms of graphene. Homogeneous doping (~8 at%) was verified by Raman mapping. Interestingly, doped-graphene becomes more transparent due to widening of graphene bandgap.

Arc-discharge approach is another technique to create reactive heteroatom radicals for graphene doping. Li *et al.* prepared N-doped multi-layered graphene sheets (1 at%) by DC arc-discharge using NH_3 as the buffer gas.[114] NH_3 not only acts as N precursor but also suppresses the formation of fullerenes by terminating the edge-sited dangling C bonds with the decomposed reactive hydrogen. In addition to NH_3, H_2 plus B_2H_6, boron-stuffed graphite, and H_2 plus pyridine have also been utilized as the heteroatom precursors in arc-discharge process for the synthesis of B- and N-doped graphene (but with low doping level of <3 at%).[115] Shen *et al.* developed a direct-current arc-discharge method for the preparation of F-doped multi-layered graphene sheets.[116] A hollow graphite rod filled with powdery graphite fluoride was used as the anode and a discharge current of 140 A was applied. The resultant F-graphene is super-hydrophobic containing ~10 wt% fluorine. While suffering from low doping levels and difficulty to obtain single-layered doped graphene, the feasibility for mass-production and preservation of high crystalinity of graphene are the main advantages of the arc-discharge techniques.

3 The properties of heteroatom doped graphene

Invasion of heteroatoms into the perfect hexagonal carbon sheet of pristine graphene will inevitably cause structural and electronic distortions, leading to alterations (sometimes drastically)

of graphene properties, including thermal stability, charge transport, Fermi level, bandgap, localized electronic state, spin density, optical characteristics, and magnetic property. Depending on the type of dopants (with particular valence and size) and their bonding configurations, new or improved properties may arise and be beneficial for particular applications. A good understanding on how graphene properties can be tailored by heteroatom doping is critical for researchers to design and discover novel functionalities of graphene materials, and therefore further extend the range of their applications.

3.1 Group IIIa element (B)

Boron ($2s^2 2p^1$), which is the neighboring element to carbon ($2s^2 2p^2$) with only one less valence electron, is highly amenable for graphene doping. In-plane substitutional doping (i.e. in-plane BC_3) is most stable compared with out-of-plane bonding (Fig. 9a).[117] As B atom forms sp^2 hybridization in the carbon lattices, the planar structure of graphene is retained. But charge polarization exists between neighboring C atom and electron-deficient B atom. In addition, the lattice parameters are slightly altered because B-C bond (~1.50 Å) is longer than C-C bond (1.40~1.42 Å) in pristine graphene.[117-119] With lower induced strain energy, homogeneous substitutional B-doping is easier to achieve compared with in-plane N-doping.[120, 121] Despite the bond length expansion, the strong B-C bond ensures minimal compromise to the excellent mechanical properties of graphene.[122] On the other hand, B-doping introduces significant destructive effect on the thermal conductivity of graphene. Only 0.75 at% of B atoms can reduce more than 60% thermal conductivity of graphene.[122] In contrast to graphitic B-doping, bonding of B atoms at the vacancy sites will create structural distortion (thus significant changes in properties). *Ab initio*-DFT/GGA-simulations were performed to study the situation of filling a divacancy with a B atom.[119] The results suggest a new type of structural rearrangement - a symmetric disposition with a tetrahedral-like BC_4 unit, of which all dangling carbon atoms are saturated (Fig. 9c). Such special fourfold coordination configuration distorts the graphene's planar structure.

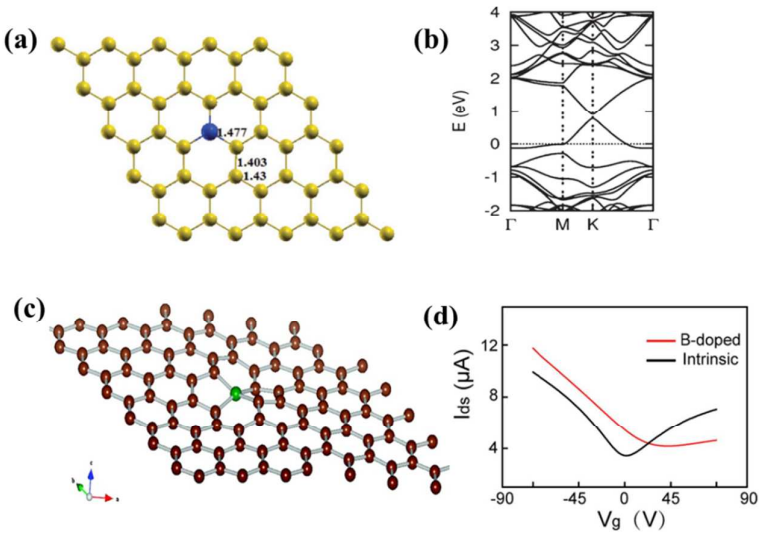

Fig. 9 (a) Substitutional doping of B (blue ball) and (b) band structure of a single B atom doped graphene sheet. Adapted with permission from ref. 117. Copyright (2013) Royal Society of Chemistry. (c) B atom in a divacancy with symmetric disposition. Adapted with permission from ref. 119. Copyright (2010) American Chemical Society. (d) Source-drain current (I_{ds}) *vs.* back gate voltage (V_g) with V_{ds} = 0.1 V of B-doped (red) and pristine (black) graphene device, respectively. Adapted with permission from ref. 36. Copyright (2010) Wiley Publishing Group.

Heteroatom doping offers possibilities for tailoring the electronic properties of graphene. The electron-deficient nature of B induces p-doping effect accompanied with a downshift of Fermi level towards Dirac point (Fig. 9b).[117] It has been predicted that the Fermi level decreases ~0.65 eV with 2 at% graphitic B and more at higher doping levels.[121] Scanning tunneling microscopy (STM) and theoretical simulation show that B-doping pulls more density of states (DOS) above the Fermi level because of hole-doping effect.[118, 123] It has been shown theoretically that a bandgap of 0.14 eV can be introduced by doping a B-atom into 50 C-atom matrix, transforming graphene from semimetal to semiconductor.[117, 124] The symmetry breaking in carbon lattice is believed to be responsible for the bandgap opening which is maximized when B-atoms are located at the same sublattice positions. Bandgap opening is also sensitively dependent on the doping concentration and the graphene thickness (number of layers).[117, 125] First principles calculations show that B or N substitution almost does not change the linear dispersion of the electronic bands within 1 eV of the Fermi level (Fig. 9b), meaning that B or N doped graphene inherits some intrinsic electronic properties of graphene.[117, 121] The anisotropy caused by B-doping, however, is not sufficient to

induce localized states and thus magnetism.[119]

As shown by a theoretical study, the remarkable transport properties of graphene preserves even at a high substitutional B/N doping level of 4.0 at%.[126] But the mobility of electrons and holes (thus conductivity) becomes asymmetric with respect to the Dirac point. This is supported by the experimental observation that B-doped CVD-graphene exhibits a high carrier mobility of 800 $cm^2 V^{-1}s^{-1}$ and a typical p-type conductive behavior with a strong asymmetry in hole and electron conduction (Fig. 9d).[36] The large Dirac point shift (~30 V) corresponds to a hole-doping concentration of ~2×10^{12} cm^{-2}. The electrical conductivity of B/N doped graphene increases with the dopant concentration at low temperature region and decreases due to elevated scattering effect from the impurity atoms at high temperature region.[127] Considering the remarkable difference between multilayer and single-layer graphene in electronic properties, Guillaume et al investigated the influence of asymmetric substitutional B/N doping on bilayer graphene.[128] A smaller doping-induced Fermi level shift is observed in bilayer because electrons and holes are shared by the neighboring carbon layers.

3.2 Group Va elements (N and P)

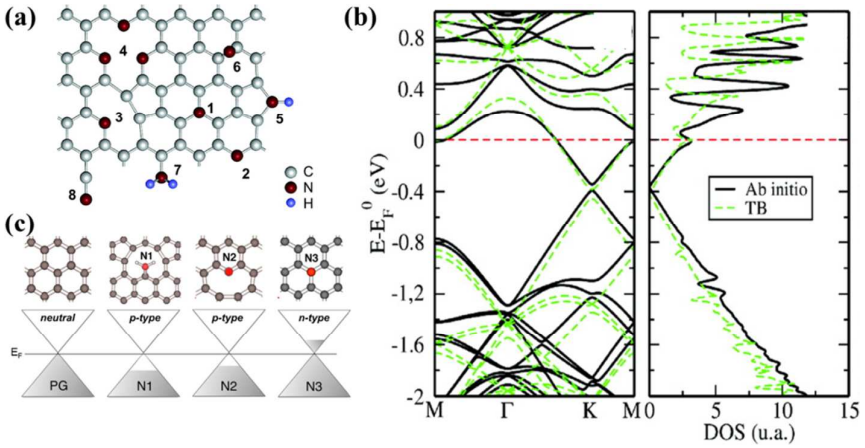

Fig. 10 (a) Possible configurations of nitrogen dopants in graphene: 1-graphitic N, 2-pyridinic N, 3-single N pyridinic vacancy, 4-triple N pyridinic vacancy, 5-pyrrolic N, 6-interstitial N or adatom, 7-amine, 8-nitrile. Adapted with permission from ref. 129. Copyright (2011) American Chemical Society. (b) Ab initio (thick black lines) and tight-binding (green dashed lines) band structures (left) and DOS (right) of a 10 × 10 graphene supercell containing one substitutional N dopant. Adapted with permission from ref. 134. Copyright (2013) American Chemical Society. (c)

Computed doping effect of N-dopant for the different bond types compared to pristine graphene. Adapted with permission from ref. 137. Copyright (2012) American Chemical Society.

N is also a neighboring element to carbon in the periodic table. The electron-rich nature of N ($1s^2 2s^2 2p^3$) makes N-doped graphene distinctly different from B-doped grpahene. The possible bonding configurations of N dopants are shown in Fig. 10a.[129] As discussed in the Synthesis Methods section, mainly three N bonding configurations exist, i.e., graphitic (or quaternary), pyridinic and pyrrolic N. Because of similar bond length of C-N (1.41 Å) to C-C (1.42 Å), pyridinic and graphitic N introduce little influence on the graphene structure. In contrast, sp^3 bonded pyrrolic N disrupts the planar structure of graphene.[130] Pyridinic N bonding configuration is most stable in the presence of monovacancy while pyridinic and graphitic N dominate in the presence of Stone-Wales and di-vacancy defects.[131, 132]

The larger electronegativity of N (3.04 in Pauling scale) than that of C (2.55 in Pauling scale) creates polarization in the carbon network thereby influencing the electronic, magnetic and optical properties of graphene.[133] N-doping opens a bandgap near Dirac point by suppressing the nearby density of states (DOS), therefore conferring graphene with semiconducting properties (Fig. 10b).[134, 135] The semiconducting behavior of N-doped graphene depends on the doping configurations. For graphitic N, three valence electrons of nitrogen form three σ-bonds with neighboring carbon atom; one electron is engaged in π bond formation; and the fifth electron partially involves in the π*-state of conduction band. Each graphitic N can contribute ~0.5 electron to the π network of graphene lattice, resulting in an n-doping effect. [136] In comparison, pyridinic and pyrrolic N form at defects sites and these defects impose p-doping effect by withdrawing electrons from the graphene sheet (Fig. 10c).[137]

Liu group demonstrated graphitic-N dominated CVD-graphene with n-type behaviour and carrier mobility of 200-450 $cm^2\ V^{-1}\ s^{-1}$.[135] Li group reported crossover behaviour from p-type to n-type with increasing N-doping level, even the dominant species are pyridinic and pyrrolic types.[138] Schiros *et al.* attributed this phenomenon to the hydrogenation of pyridinic and pyrrolic N, which transformed them from p into n type.[137] Usachov *et al.* reported a bandgap opening of ~0.3 eV and charge-carrier concentration of ~8 x 10^{12} cm^{-2} induced by 0.4 at% doping of graphitic N.[129] Sodi *et al.* theoretically showed that, in contrast to doping at the basal plane, edge functional

groups make little difference to the band structure of graphene.[139] As shown by Ouerghi *et al.*, only 0.6 at% graphitic N-doping results in a large carrier concentrations of 2.6 x 10^{13} cm^{-2} (4 times higher than that of pristine graphene) while pyridinic and pyrrolic N exert little influence.[140]

N doping has also been proved to be powerful to tune the work function of graphene materials, which is instrumental for devices such as organic field effect transistor (OFET) and light emitting diodes (LEDs). Schiros *et al.* calculated the work function of pristine graphene (4.43 eV) and graphene doped with graphitic (3.98 eV), pyridinic (4.83 eV), and hydrogenated pyridinic (4.29 eV) N.[137] The change of work function is caused by the electron donating or accepting nature of each N bonding configuration. Consistently, Kim and co-workers confirmed the reduction of work function by graphitic N-doping using ultraviolet photoelectron spectroscopy.[141] Contradicting to the theoretical predication, Lin group showed that pyridinic N reduces the work function of CVD graphene.[142] This discrepancy could be due to hydrogenation of pyridinic N.[137]

More recently, creation of magnetic moment on graphene by heteroatom doping attracts great research interest for spintronic applications. Due to the lack of nonbonding electrons, graphitic N is not able to generate magnetic moment. Although both pyrrolic and pyridinic N have a nonbonding electron pair, only pyrrolic N can form π and π* state which leads to spin polarization. Therefore, pyrrolic N can create strong magnetic moment while pyridinic N only has weak effect.[143] Chen *et al.* theoretically demonstrated that each pyrrolic N doped at edge sites of graphene nanoribbons (GNR) produces a magnetic moment of 0.95 μB while a pyridinic N at edges creates a magnetic moment of 0.32 μB. [144]

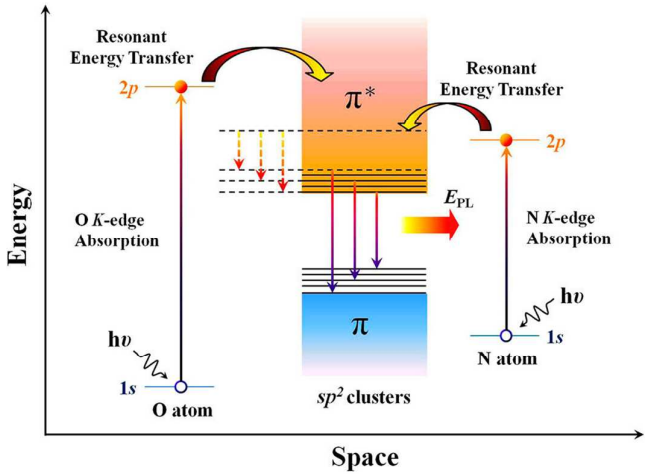

Fig. 11 Possible mechanism of photoluminescence enhancement by resonant energy transfer from N and O dopants to the sp^2 clusters in the GNFs matrix. E_{PL} stands for the enhanced PL emission. Solid and dotted lines represent radiative (E_{PL}) and nonradiative (low and broad PL) relaxation processes, respectively. Adapted with permission from ref. 145. Copyright (2012) American Chemical Society.

The N doping can also tailor the optical properties of graphene sheets. Chiou *et al.* demonstrated the influence of N-doping on the photoluminescence (PL) property of graphene nanoflakes (GNF).[145] When excited, the electrons of doped N can transfer energy to the π* state of sp^2 cluster of GNF. Therefore, a larger amount of energy is released when electrons fall from π* back to π state, leading to a higher intensity PL (Fig. 11). As demonstrated by Kim *et al.*, pyrrolic, pyridinic and graphitic N all blue-shift the PL peak while only graphitic N is able to enhance the intensity.[146] But Tang's group reported that with 3.05 at% pyridinic-N PL emission of rGO is quenched by 76% possibly because of intramolecular energy transfer between doped N and graphene sheet.[147]

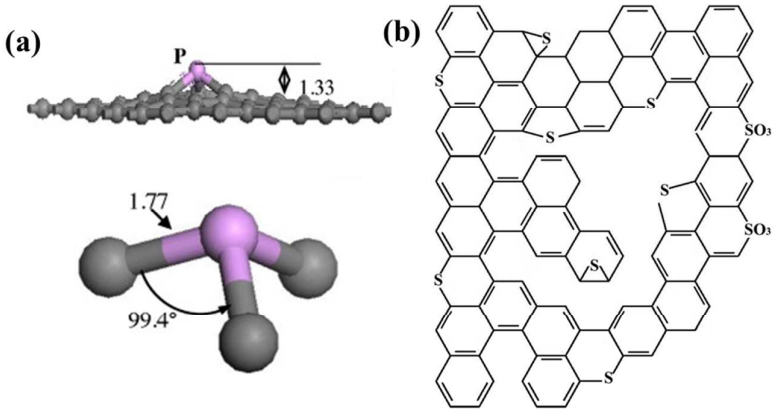

Fig. 12 (a) Optimized geometrical structure of P doped graphene. The gray and pink ball represents carbon and phosphorus atoms, respectively. The bond distances are in angstroms. Adapted with permission from ref. 148. Copyright (2013) Elsevier Publishing Group. (b) Typical configuration of S-doped graphene. Adapted with permission from ref. 82. Copyright (2012) American Chemical Society.

As P is larger than N, P-doping causes more structural distortion. By transforming the sp^2 hybridized carbon into sp^3 state, P can form pyramidal like bonding configuration with three carbon atoms. In such configuration, P overhangs from the graphene plane by 1.33Å accompanied

with 24.6% increase in P-C bond length with respect to C-C bond length of pristine graphene (Fig. 12a).[148] Unlike N, the electronegativity of P atom (2.19) is significantly lower than C atom (2.55),[149] therefore the polarity of C-P bond is opposite to that of C-N bond. And compared with N-doping, distinct effects by P-doping may also arise from the additional orbital of P ($3s^2 3p^3$). Hirshfeld population analyses show that P can transfer 0.21 e to graphene sheet[148] and graphitic N transfers 0.5 e, suggesting the stronger ability of N for electron donation[150]. Contrarily, it has been shown that P-doped bi-layer graphene exhibits prominent n-type behaviour with 5 times higher electron mobility than pristine bi-layer graphene while N-doped bi-layer graphene shows weaker n-type behavior and lower mobility than pristine graphene.[151] The same study also shows that, unlike N-induced n-doping, the n-type behavior of P-doped graphene retains in the oxygen atmosphere. The discrepancy between the theoretical prediction and experimental observation might be due to that n-doping from graphitic N is partially neutralized by the co-existed electron-accepting pyridinic and pyrrolic N.

A theoretical investigation suggests that bandgap opening positively depends on the P-doping concentration and a bandgap of 0.3~0.4 eV is resulted with P doping level of 0.5 at%.[152] Similar to N-doping, P-doping can also induce magnetic moment. Zhao *et al.* found that the magnetic moment of P-doped graphene is ~1.02 μB due to the symmetry breaking of graphene π-electron frame work.[148] This value is in good accordance with the DFT calculation (1.05 μB) reported by Dai and Yuan.[153] P-doping is more potent than N-doping in inducing magnetic moment.

3.3 Group VIa elements (O and S)

VIa group is also known as the oxygen family, among which oxygen is the most electronegative element. Substitutional doping of O atom is impossible because of its strong electronegativity and large size. Graphene oxide (GO), usually oxidatively exfoliated from graphite powder, is the mostly studied graphene derivative. Having epoxyl (C-O-C) and carbonyl (C=O) groups, GO and its reduced form (rGO) can be regarded as O-doped graphene. Covalent attachment of oxygen groups transforms sp^2 into sp^3 hybridization state, accompanied by local distortions of graphene planar structure. The extensive presence of localized sp^3 domains gives rise to bandgap opening,[154, 155] and they together with defects make GO poorly or non-conductive. Excellent hydrophilicity makes GO suitable for solution processes.

It is generally pictured that GO sheet bears hydroxyl and epoxyl groups on its basal plane, and carboxyl and carbonyl groups at the edges.[156] As a non-stoichiometric compound, the properties of GO highly depend on the abundance and composition of different types of oxygen groups which are specific to synthetic processes and post-synthesis treatments.[13, 157] Intriguingly, the chemistry of GO changes in the ambient condition, for example, epoxyl groups may evolve to hydroxyl groups in the presence of hydrogen.[158-160] Acidic and oxidative nature of abundant oxygen functionalities allows GO to function as a mild and green oxidant and catalyst. For example, GO has been reported to be capable of oxidizing substituted *cis*-stilbenes to their corresponding diketones, and facilitating oxygen activation reaction.[161-163] As GO and rGO have already been thoroughly discussed in a number of review articles,[13, 164, 165] in this article, we place more emphases on other heteroatom doping.

S shares similar doping configurations as O, e.g., C-S-C, C-SO_x-C (x=2,3,4) and C-SH (Fig.12b).[82] C-S bond (1.78 Å) is ~25% longer than that of C-C bond.[166] Consequently, curved carbon nanostructure (e.g., carbon nanotube) favors S-doping more than the flat graphene. A theoretical study proposes that S-doping on graphene occurs in two steps: formation of defect sites and S=S bond rapture, and depending on the doping level the resultant graphene sheet can become a small-band-gap semiconductor or more metallic than pristine graphene.[167] Poh *et al.* experimentally measured the resistivity of S-doped graphene thermally exfoliated from graphite oxide in the presence of S-precursor.[78] In general, S-doped graphene is more resistive than pristine graphene because of the free carrier trapping caused by sulfur and oxygen functionalities.

Unlike B, N, and P, negligible polarization (or charge transfer) exists in C-S bond because of the similar electronegativity of S (2.58) and C (2.55).[168] On the other hand, in contrast to the zero spin density of pristine graphene, the mismatch of the outermost orbitals of S and C induces a nonuniform spin density distribution on S-doped graphene, which consequently endows graphene with catalytic properties useful for many applications (e.g., oxygen reduction reaction - ORR).[82, 83] Using first-principles calculations, Jeon *et al.* found that covalently bonded S and oxidized S at both zigzag and armchair edges of graphene nanoplates (SGnPs) obtained from ball milling can induce significant spin density increase.[82] In addition, oxidization of SGnPs further enhanced their catalytic activity, accompanied by 5~10 times increase of magnetic moments. The same study also showed that the highest occupied molecular orbital (HOMO) and lowest unoccupied molecular

orbital (LUMO) of graphene are strongly polarized by edge-sited S dopants, leading to high catalytic activity towards ORR. In contrast to the intensive study on O- and S-doping, there are only a few reports on Se-doping.[80] The properties of Se-doped graphene remain largely unexplored.

3.4 Group VIIa elements (F, Cl, Br and I)

As is well known, halogens possess higher reactivity than group IIIa-VIa elements. As halogen-doping transforms sp^2 carbon bonding to sp^3 state, drastic distortions on geometric and electronic structures of graphene will be resulted. As F is one of the most reactive elements, F-bonding is strong and inert. F-C bond on F-doped graphene sticks out the basal plane (Fig. 13a)[111] and it stretches the C-C bond length to 1.57~1.58 Å.[169] First-principles calculations suggest that the high affinity of F towards C enables negative chemisorption energy of F on graphene even at full coverage of F atoms ($[CF]_n$ which is called fluorographene).[170] For fluorographene, F is covalently bonded to sp^3 C and graphene sheet is buckled as F attachment alternates on both sides of graphene sheet (i.e., basal plane is sandwiched by two F-layers). Fluorographene has attracted a great deal of attention because of its extraordinary mechanical strength, high thermodynamic stability and superb chemical inertness.[169, 170] These properties promise the use of fluorographene, for examples, as lubricant and battery additive. Fluorographene is the thinnest insulator because of its wide bandgap of ~3 eV resulting from high degree of sp^3 bonding of carbon atoms (Fig. 13b).[169, 171, 172]

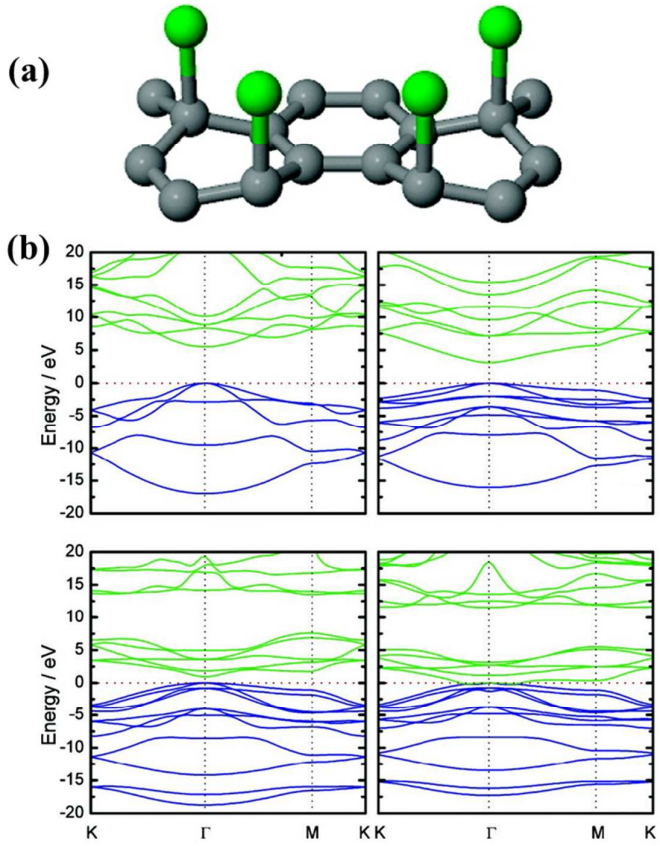

Fig. 13 (a) Schematic illustration of partially fluorinated or chlorinated graphene structure. Adapted with permission from ref. 111. Copyright (2011) American Chemical Society. (b) The electronic band structure of CH, CF, CCl, and CBr along lines connecting the high-symmetry points K, Γ and M in the Brillouin zone. The zero-energy level has been set to the valence band maximum. Adapted with permission from ref. 169. Copyright (2010) Wiley Publishing Group.

F-doping graphene can be employed as semiconductors with a bandgap tunable by F-coverage[98] and with luminescence ranging broadly from ultraviolet to visible light region[173]. Obtained by exposing only one-side of CVD graphene to xeon difluoride, single-sided F-doped graphene (25% F coverage, C_4F) is optically transparent with a band-gap of 2.93 eV and over 6 orders of increase in resistance as compared with pristine graphene[171]. And F-doping increases hydrophobicity of graphene.[116]

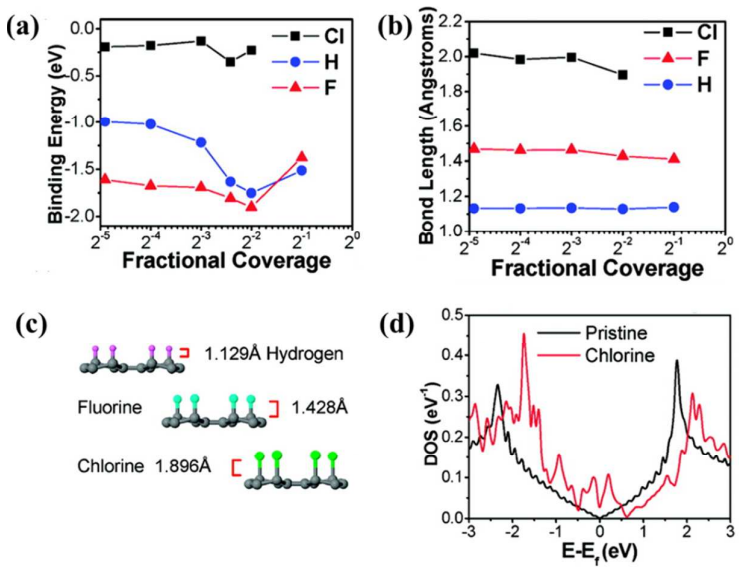

Fig. 14 (a) Binding energies and (b) bond lengths of the C-X bond (X = Cl, H, F) as functions of coverage, based on ab initio simulations. (c) Atomistic structures and bond lengths of C-X. (d) Calculated DOS of graphene with a 1/30 coverage of Cl atoms in comparison with that of pristine graphene as a function of energy E - E_F, where E_F is the Fermi energy. Adapted with permission from ref. 111. Copyright (2011) American Chemical Society.

In the case of Cl-doped graphene, *ab initio* simulations show that Cl atoms on graphene have lower binding energy and longer bond length than that of F and H, suggesting that the covalent Cl-C bond is less stable than C-F and C-H bonds (Fig. 14a-c).[111] Because of the long bond length, Cl-doped graphene (1.1-1.7 nm) is thicker than F-doped graphene.[113] In addition to the similar bonding arrangement as F (Fig. 13a), Cl can interact with C *via* forming charge-transfer complex, covalent bonding, and physical absorption as suggested by DFT calculations.[130] 25% coverage of covalently bond Cl (C_4Cl) creates a bandgap of 1.4 eV. At full coverage of Cl, Br and I, non-covalent interaction is more stable.[174, 175] Full coverage of Cl (like fluorographene) is controversial. It has been theoretically proposed that alternative covalent bonding on both sides allows full Cl coverage and even at full coverage the graphene bandgap is only opened to ~1 eV (Fig. 13b).[169] But Sahin *et al.* reported that dense decoration of Cl on graphene surface leads to desorption of Cl in the form of Cl_2 due to stronger Cl-Cl interaction.[176]

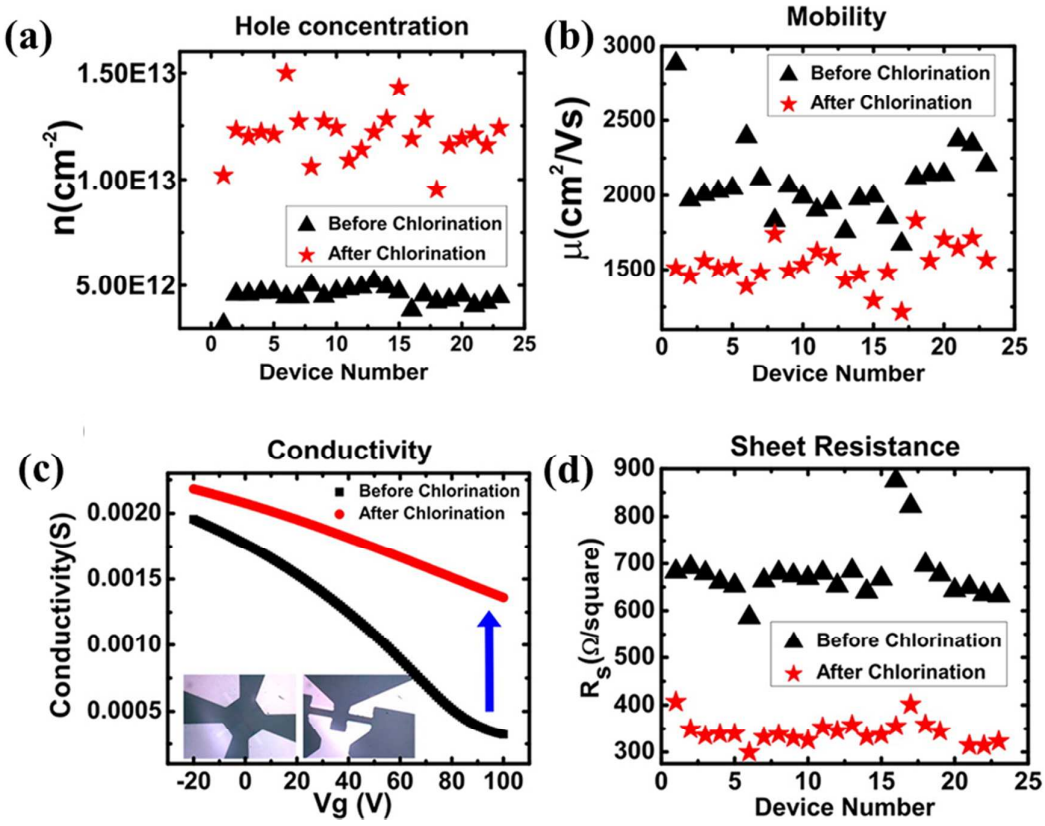

Fig. 15 Chlorination changes the transport properties of graphene: (a) carrier concentration, (b) mobility, (c) electrical conductivity, (d) sheet resistance. Adapted with permission from ref. 112. Copyright (2013) American Chemical Society.

Cl is a p-dopant (Fig. 14d). Zhang *et al.* successfully synthesized Cl-doped graphene with a high Cl coverage of 45.3% (close to C_2Cl), which was stable over one week under ambient conditions.[112] Hall-effect measurements reveal the p-doping effect and a high hole concentration of 1.2 $\times 10^{13}$ cm^{-2} (increase of ~3 times) (Fig. 15). In comparison with the carrier mobility decrease of F-doped graphene from 1060 cm^2 V^{-1} s^{-1} to about 5 cm^2 V^{-1} s^{-1},[171] Cl-doping preserves a high carrier mobility of 1535 cm^2 V^{-1} s^{-1}.[112] In addition, Cl-doping enhances the conductivity of graphene by 2 times (Fig. 15). Owing to low binding energy, Cl-doping and Br-doping start to decompose at low temperature (<400 °C) and completely evaporate at >600 °C.[99]

In contrast to the extensive research efforts spent on F- and Cl-doping, there are only a few theoretical and experimental reports on Br- or I-doped graphene. This is due to thermodynamic instability correlated with their large sizes and low electronegativity (F = 3.98,

Cl = 3.16, Br = 2.96 and I = 2.66). Unlike F and Cl, the large-sized halogen atoms (Br and I) likely interact with graphene only *via* physisorption or charge-transfer complex formation, without disrupting the sp^2 carbon network.[174, 177] As shown in Fig. 13b, brominated graphene is an indirect gap material with almost zero bandgap. In comparison, hydrogenated, fluorinated and chlorinated graphene materials are direct bandgap materials.[169] And DFT studies reveal the metallic behaviors of Br- or I-doped graphene materials.[169, 174] The electronegative and chemically reactive properties of I make it easily aggregate to form linear polyiodide anionic species (e.g. I_3^- and I_5^-) on the graphene surface.[46, 85]

3.5 Other dopants

Graphene hydrogenation *via* sp^3 C-H bond can transform zero bandgap graphene into wide-gap semiconductor.[178, 179] Many studies have been conducted on the structural, electronic and magnetic properties of fully or partially hydrogenated graphene.[180-182] But because of the small difference in electronegativity between C and H, C-H bond is essentially non-polar and thus non-reactive. This largely limits the practical applications of hydrogenated graphene materials.

Doping of metallic atoms has rarely been demonstrated experimentally. This is probably because the binding energy between these elements with graphene is much lower than their cohesive energy. Consequently, they tend to form clusters instead of being uniformed doped on graphene surface.[183] In addition, large-sized metal atoms can create large local curvature favoring chemisorption of small molecules from the ambient (e.g., H_2O, O_2, NO), which greatly limits the practical applications of such doped graphene.[184, 185]

Silicon (Si), which belongs to the same group as C, is a tetravalent metalloid. The much longer bond length of Si-C (1.75 Å) with respect to C-C bond forces Si atom to protrude from the graphene plane, accompanied with remarkable distortion of graphene planar structure. The created disorders make Si-doped graphene promising as metal-free catalyst for CO oxidation,[186] ORR,[187] NO and NO_2 reduction[188, 189]. However, the experimental reports on Si-doped graphene are rare. This may, at least in part, attributable to the strong chemisorption of ambient molecules[190] which unavoidably change the intrinsic properties of Si-doped graphene.

3.6 Co-doping

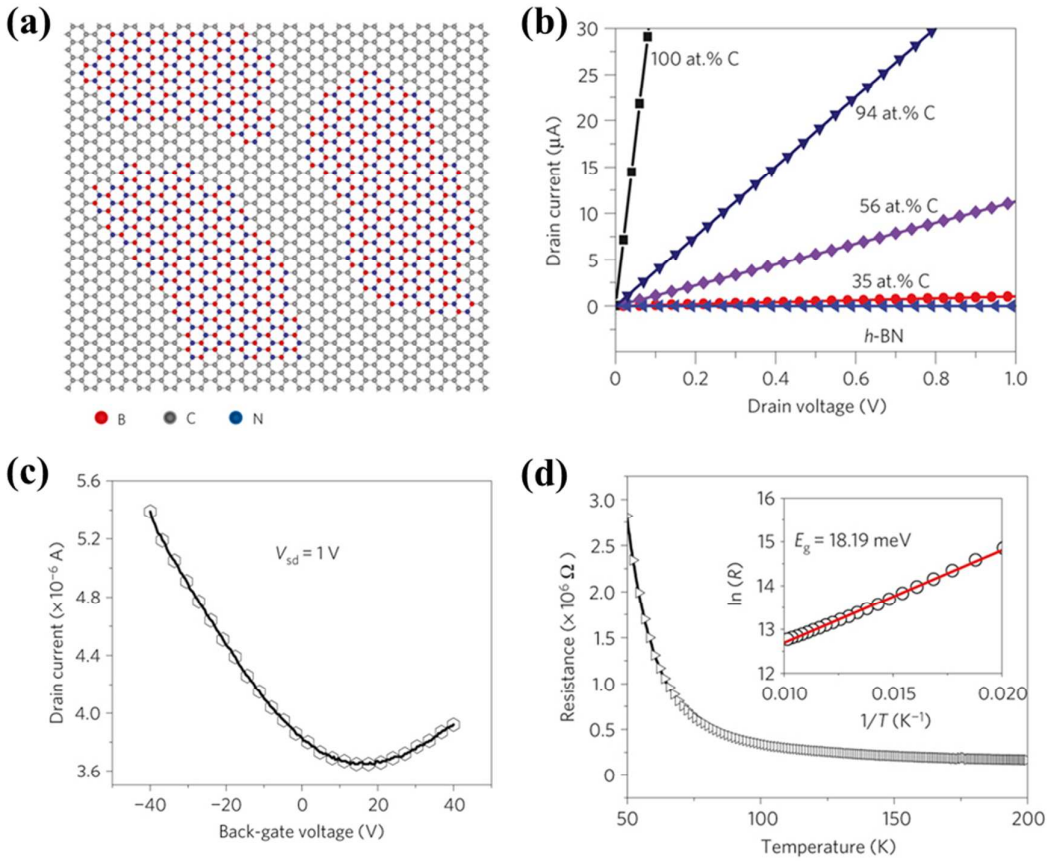

Fig. 16 (a) Atomic model of the *h*-BNC film showing hybridized *h*-BN and graphene domains. Scale bars: 2 nm. (b) Current–voltage (*I*–*V*) characteristics of as-grown BNC with different percentages in carbon measured at room temperature. (c) The drain current as a function of the voltage applied to the back gate for a 7-μm-wide BNC ribbon with 40% carbon. The drain–source voltage is fixed to 1 V. (d) Resistance *vs*. temperature curve for a typical *h*-BNC ribbon with a width of 5 μm and a length of 11μm. The inset shows ln(*R*) as a function of T^{-1} in the temperature range from 50 to 100 K. Adapted with permission from ref. 33. Copyright (2010) Nature Publishing Group.

Co-doping of multiple species of foreign atoms may generate new properties or create synergistic effects. B and N atoms are similar in size and produce opposite doping effects on graphene. While being simultaneously doped onto graphene, boron nitride (BN) domains tend to form due to phase separation between C and BN (Fig. 16a).[33, 191-194] This is attributed to the larger binding energy of B-N and C-C than that of B-C and N-C bonds. B,N co-doping leads to four bonding configurations, i.e. C-C, B-N (dominating form), C-B and C-N with bond length of 1.42

Å, 1.45 Å, 1.49 Å and 1.35 Å, respectively.[193] Strong charge polarization exists between B and N[193, 195] which renders active surface chemistry. Thermal stability of B,N co-doped graphene is lower than N-doped graphene, but higher than B-doped graphene.[35]

Co-doping of B and N on graphene by CVD produces a sp^2 hybridized hexagonal lattice with BN domains (B/N ratio = 1) surrounded by graphitic domains.[33] The conductivity of such film (h-BNC) is tunable from insulating to highly conductive depending on the C percentage (Fig. 16b). Similar to previously reported BC_2N thin-film,[196, 197] h-BNC exhibits a p-type semiconducting behavior with electron and hole mobility of 5-20 $cm^2\ V^{-1}\ s^{-1}$ (Fig. 16c). The reduced mobility is attributed to electron scattering at the boundaries between BN and C domains. Based on the temperature-dependent resistivity of h-BNC (with 56 at% C), a small bandgap (18 meV) is predicted (Fig. 16d). Asymmetric B,N doping ($B_{7.8}N_{4.7}C_{87.5}$) gives moderate increase in bandgap (0.49 eV) because of symmetry breaking.[198] It has been shown that at appropriate B/N ratio the HOMO-LUMO energy gap of graphene may be reduced leading to enhanced chemical reactivity.[69] Both B and N doping creates a bandgap at Dirac point, but they shift Fermi level in opposite directions. Uniform B,N co-doping (although it is difficult to experimentally realize) is believed to open a bandgap at Dirac point without shifting Fermi level.[193, 199, 200] As suggested by DFT studies, the opened bandgap increases with the size of BN domains regardless of its shape.[195]

In contrast, random and scattered distribution of foreign atoms is observed in the case of S,N or P,N co-doping.[45, 201] Crosstalks between the co-dopants may affect their bonding configurations. For example, co-doping of P may promote pyridinic bonding of N on graphene.[201] Pyrrolic N dominates in N-doped graphene whereas co-doping of S makes graphitic N dominant.[45]

4 Applications

Doping by a range of heteroatoms with varying configurations and doping levels endows graphene with a wide spectrum of new properties, for examples, bandgap opening, charge polarization between heteroatom and C atom, magnetic moment, hydrophilicity, increased spin density, catalytic activities, etc. Doped graphene materials are therefore useful for various applications including energy storage, energy conversion, sensing, and gas storage (Table 2).

Table 2 Summary of applications of heteroatom-doped graphene

Materials	Advantages of doping effect	Ref.
B/ N/ P doped graphene	Enhancedelectrochemical activity;lower charge-transfer resistance; better sheet-to-sheet separation;improved conductivity than GO precursors.	203, 206, 207
B, N co-doped graphene		101
N-doped graphene/MnO_2		211
B/ N/ P doped graphene	Achieving balance between Li binding and diffusion; enable abundant and uniform loading of metal oxide nanoparticles.	59, 224
N, S co-doped graphene		225
N doped graphene-SnO_2 /MnO /TiO_2 /VO_2 /Zn_2GeO_4 /α-Fe_2O_3		106, 226-230
B/ N/ P/ S/ halogendoped graphene	Induced charge polarization and spin density enhances oxygen adsorption and cleavage;enable abundant and uniform loading of metal nanoparticles.	43-47, 51, 53
N, B/ N, P/ N, S co-doped graphene		69, 80, 201
N doped graphene-Pt NW/ PtRu		81, 251
B/ N/ F doped graphene	Increases the catalytic activity of DSSC counter electrode; endowsgraphenewith p or n doping effect; increasesgraphene work function.	32, 254, 257
B/ N/ P/ Si/ S doped graphene	Facilitates charge transfer, analyte adsorption and activation; assists anchoring of functional moieties or molecules; opens graphenebandgap; induces charge polarization.	39, 262, 263, 269, 275
B, N/ S, N/ Si, N co-doped graphene		261, 266, 272
B/ N doped graphene	Increases binding affinity towards gas molecules;enable abundant and uniform loading of metal nanoparticles.	277, 281, 282

4.1 Supercapacitors

Due to its high power density and long lifecycle, supercapacitors have been insensitively researched as energy storage devices. Graphene, which has the highest specific surface area, offers large electric double-layer capacitance (EDLC). However, the chemically insert pristine graphene is not able to provide electrochemical capacitance (pseudocapacitance). Hence, doped graphene materials are promising for supercapacitors because of preserved large EDLC, improved wettability, and existence of pseudocapacitance.[202]

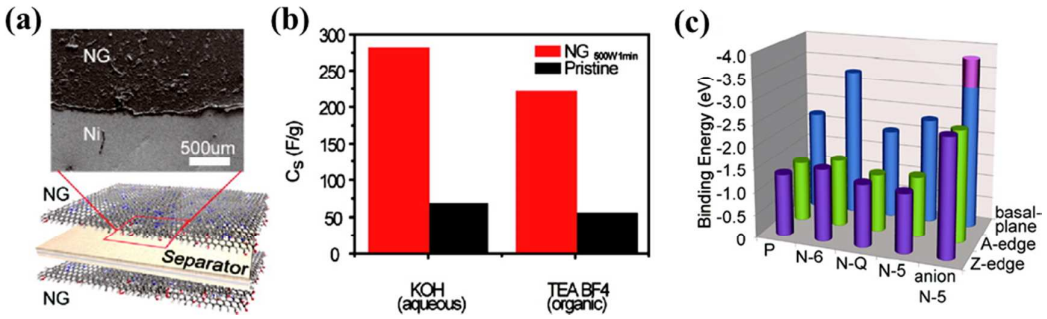

Fig. 17 Ultracapacitors based on N-doped graphene and their electrochemical testing. (a) A schematic illustration of the assembled supercapacitor structure alongside a scanning electron microscopy image showing a top view of the device. (b) The specific capacitances measured in aqueous and organic electrolytes. (c) The binding energies between potassium ions and N-configurations at basal planes and edges, which were calculated by first-principles DFT. "P, N-6, N-Q and N-5" in the horizontal axis indicates "pristine", pyrrolic N, pyridinic N and graphitic N, respectively. Adapted with permission from ref. 108. Copyright (2011) American Chemical Society.

It has been shown that the abundant oxygen groups on rGO enhance its specific capacitance to 189 F g^{-1}.[203] Compared with O-doped graphene, graphene materials doped by B, N and P are more advantageous with better conductivity, stability, chemical reactivity, sheet-to-sheet separation. A porous B-doped graphene structure synthesized by annealing frozen GO-boric acid composite shows a specific capacitance of 281 F g^{-1}.[60] N-doped graphene hydrogel (5.86 at% N with dominant pyrrolic N) synthesized by hydrothermal method gives a large specific surface area of ~ 1500 m^2 g^{-1} and a high specific capacitance of 308 F g^{-1}.[100] The same study also showed that the capacitive performance of N-doped graphene not only depends on N content but also doping configurations. Graphitic and pyridinic N can improve the wettability of doped graphene because of their large dipole moments. And graphitic N can facilitate electron transfer, whereby improving the capacitive behavior by lowering the charge-transfer resistance of the electrode at high current density.[108, 204] Being electrochemically active in alkaline aqueous solution, pyridinic and pyrrolic N offer high pseudocapacitance.[100] At optimized balancing in N bonding configuration and doping level, a hydrothermally synthesized N-doped graphene (10.13 at%) achieves a specific capacitance of 326 F g^{-1} and excellent cycling stability (99.85% columbic efficiency after 2000 cycles).[205]

Jeong *et al.* fabricated a N-doped graphene-based flexible (wearable) supercapacitor which exhibits 4 times larger capacitance than the pristine graphene-based counterpart, in both aqueous and organic electrolytes (Fig. 17).[108] Theoretical calculations suggest that pyridinic N at the basal plane plays a major role for capacitance improvement due to its large binding energy with K^+. On the other hand, the strong ionic bonding between negatively charged pyrrolic and K^+ is predicted to be disadvantageous for reversible charge-discharge process (Fig. 17). Fan *et al.* synthesized N-doped graphene (8.7 at%) hollow structure by thermal annealing of layer-by-layer composited GO, PANI and polystyrene nanosphere.[206] Attributable to the synergistic effect of N-doping and hollow-sphere structure, it exhibits a high specific capacitance even at high current density (381 F g^{-1} at 1 A g^{-1}; 282 F g^{-1} at a high current density of 20 A g^{-1}) and outstanding cycling stability (96% retention after 5000 cycles).

Rajalakshmi *et al.* prepared P-doped graphene by annealing rGO with phosphoric acid at 220 °C.[207] Working as the supercapacitor electrode in 1 M H_2SO_4 electrolyte, it offers a much higher capacitance (367 Fg^{-1} at scan rate 5 mV s^{-1}) than RGO control.[207] Phosphorus on graphene is believed to assume the oxidized form and produces pseudocapacitance. S and halogen atom doping are also expected to enhance the capacitance of graphene-based electrodes. However, their practical applications on this regard are hindered by the complicated synthesis process, limited doping level and/or low yield. In addition, the pseudocapacitive behaviors from these dopants are unclear. A few S-doped activated carbon materials have been reported for supercapacitor applications, and sulfone and sulfoxide species formed have been proposed to participate in the redox faradic reactions during charge-discharge process.[208, 209]

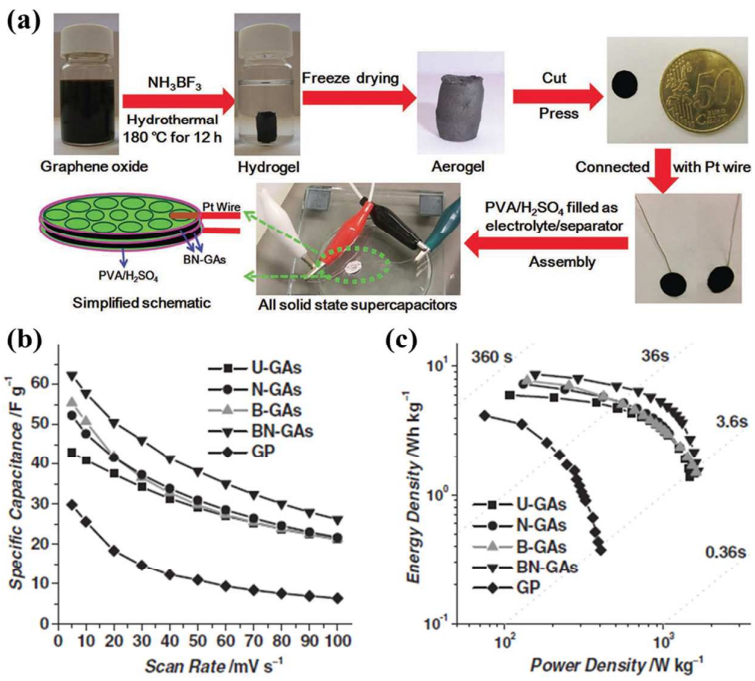

Fig. 18 (a) Fabrication of all-solid-state supercapacitor (ASSS) based on B,N-GAs that were produced by a combined hydrothermal process and freeze-drying process. (b) Specific capacitance of undoped GAs (U-GAs), N-GAs, B-GAs, BN-GAs, and graphene paper (GP) based ASSSs based on two-electrode mass as a function of scan rates from 1 to 100 mV/s. (c) Ragone plot of ASSSs based on U-GAs, N-GAs, B-GAs, B,N-GAs and GP. Adapted with permission from ref. 101. Copyright (2012) Wiley Publishing Group.

Wu *et al.* synthesized 3D B,N co-doped graphene aerogel (BN-GA, ~0.6 at% B and ~3.0 at% N) as an additive-free monolithic composite for all-solid-state supercapacitor (Fig. 18).[101] This electrode (with capacitance of 239 F g^{-1}) outperforms the counterpart electrodes without doping or doped with only B or N because of the synergetic effects between the two co-dopants. The solid-state supercapacitor equipped with such electrode achieves a high energy density of ~8.7 Wh kg^{-1} and power density of 1650 W kg^{-1}. O, N and Cl triply-doped rGO (16.36 at% O, 1.46 at% N mainly as pryidinic N, 1.1 at% Cl mainly as C-Cl or C-Cl=O) has been prepared by anode polarization of rGO film in nitrogen-deaerated 1 M KCl solution.[210] These electron-rich dopants largely increase the electrode capacitance as compared with rGO based electrode. Heteroatom doping not only enhances the capacitance of graphene materials, but also facilitates uniform and abundant loading of pseudocapacitive metal oxides *via* serving as the nucleation and anchoring

sites. Yang *et al.* synthesized a composite of N-doped graphene and ultrathin MnO_2 sheet by hydrothermal method and found a specific capacitance increase from 218.8 to 257.1 F g^{-1} and improved cycling stability after N-doping.[211]

4.2 Lithium ion batteries

Lithium ion batteries (LIB) are energy storage devices of high energy density. But they have relatively low power density and poor cycling stability. Pristine graphene is not suitable for Li storage due to 1) its low binding energy towards Li atoms (hence adsorbed Li atoms tend to cluster on graphene surface) and 2) high energy barrier for Li to penetrate through graphene sheet.[212, 213] The existence of defects enables Li penetration and prevents Li clustering due to strong interaction between Li and defect sites.[213, 214] On the other hand, the abundant defect sites not only compromise the mechanical robustness and electrical conductivity of graphene, but also limit Li's lateral diffusion.[215]

Heteroatom doping could be instrumental to optimally balance Li storage and diffusion for graphene-based electrodes.[216] Partial density of state (PDOS) study suggests that Li atom as a potent electron donor is fully ionized on graphene and interacts with graphene mainly by ionic bonding.[217] Graphene substitutionally doped with B atoms is an electron-deficient system which is desirable for improving the storage capacity of electron-donating Li.[217, 218] However, the enhanced binding energy between Li and B-doped graphene limits Li diffusion (thus delithiation process).[217, 219] In contrast, graphene doped with electron-rich graphitic N shows more efficient delithiation because the electrostatic repulsion between N and Li.[212, 217] But this comes with a price of reduced Li storage capacity due to lowered binding energy.[220] Taken together, graphitic B doping promotes LIB capacity whereas graphitic N doping improves charge/discharge rate performance. Both graphitic doping is not able to enhance the penetration of Li through graphene sheets (perpendicular diffusion).[213]

Pyridinic and pyrrolic N formed at the edges and defect sites can promote perpendicular diffusion of Li.[213, 221] In addition, Cao *et al.* showed theoretically that pyridinic and pyrrolic N have higher binding energy with Li than that of graphitic N, which is favorable for increasing the storage capacity.[216] On the other hand, the strong coulombic attraction between pyridinic/pyrrolic N and adsorbed Li^+ hinders the delithiation process.[213] A theoretical study shows that N-doping at

divacancy defects facilitates the perpendicular penetration while doping at both monovacancy and divacancy has desired binding energy to optimally balance binding capacity and dilithiation of Li.[213]

Experimental investigations have been conducted to explore the potential of B or N doped graphene as LIB anode. Reddy *et al.* reported a CVD-grown N-doped graphene (9.0 at%) anode that achieves a higher reversible discharge capacity (0.05 mAh cm^{-2}) than that of pristine graphene.[37] The improved performance is benefited from the dominant pyridinic N species and N-doping induced topological defects. Wang *et al.* synthesized N-doped graphene (~2 at%) by thermal annealing GO in NH_3 which offers a high reversible capacity of 900 mAh g^{-1} (5 times higher than that of pristine graphene) with excellent rate performance.[68] Using a similar annealing method, Wu *et al.* prepared B-doped (0.88 at%) and N-doped (3.06 at%) graphene, which gave high reversible capacity of 1549 or 1043 mAh g^{-1} with superior high rate performance, respectively.[59] These B-doped and N-doped graphene anodes also exhibit excellent energy (~34.9 kW $kg_{electrode}^{-1}$ and ~29.1 kW $kg_{electrode}^{-1}$) and power density (~320 Wh $kg_{electrode}^{-1}$ and ~226 Wh $kg_{electrode}^{-1}$), which are much higher to that of pristine graphene. The improved performance is attributed to increased conductivity, chemical reactivity, and wettability resulting from heteroatom doping.

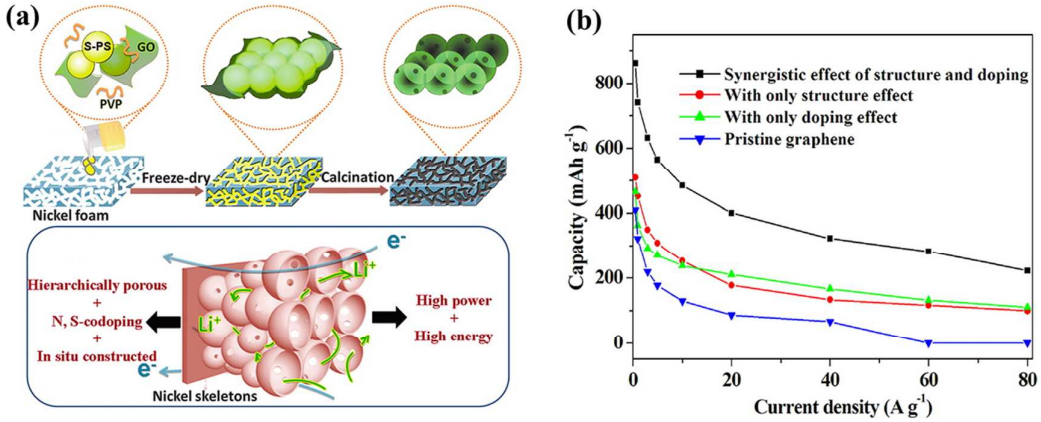

Fig. 19 a) Schematic illustration of synthesis procedures of 3D N,S co-doped graphene hieratical structure. b) Comparison of lithium storage performance of pristine graphene and graphene with different effects. Adapted with permission from ref. 225. Copyright (2013) American Chemical Society.

Doping of other heteroatoms (e.g. O, Si, P, and S and halogen atoms) has also been reported to enhance LIB performance. The oxygen groups (e.g. carbonyl, ester, carboxylic, epoxide and hydroxyl groups) on GO or rGO can enhance the capacity of LIB *via* Faradaic reaction with Li, for example, $Li^+ + C=O + e^- \leftrightarrow C\text{-}O\text{-}Li$.[222, 223] However, their instability at high current density compromises the rate performance of LIB.[59] Theoretical calculations show that binding of Li to B, Si, and P dopants (but not N and S) are energetically favored.[212] Hou *et al.* reported a P-doped graphene (1.32 at%) anode with a higher reversible capacity (~ 460 mAh g^{-1}) than that of pristine graphene.[224] The authors attributed this improved performance to the topological defects caused by P doping. Wang *et al.* fabricated 3D N,S co-doped graphene hieratical structure (4.2 at% N and 0.94 at% S) as LIB anode (Fig. 19).[225] Owing to the synergistic effects between the 3-D structure and co-dopants, such LIB exhibits excellent rate performance and a high reversible capacity of 1137 mAh g^{-1} which is ~3 times of the theoretical capacity of graphite and much higher than pristine graphene.

Heteroatom doping can be utilized for anchoring of nanostructured metal oxides (e.g. SnO_2,[226] MnO,[227] TiO_2,[228] VO_2,[106] Zn_2GeO_4[229] and α-Fe_2O_3[230]) in order to improve LIB performance. For example, a sandwich paper of N-doped graphene (8 at%) and SnO_2 provides a higher capacity (918 mAh g^{-1}) than the pure SnO_2 nanoparticles or graphene paper.[226] In addition to serving as the conducting network, the intercalated N-doped graphene sheets also prevent the aggregation of SnO_2 nanoparticles and provide an elastic buffer space for the volume change of SnO_2 nanoparticles during Li-ion insertion/extraction process which is crucial for high rate performance and cycling stability.

4.3 Fuel cells

Developing state-of-the-art electrocatalyst system with mass-produced and cost-effective materials is pivotal to underpin the industrial operation of fuel cells, in which the sluggish cathodic oxygen reduction reaction (ORR) is often the rate limiting step. Theoretical and experimental studies have shown that pristine graphene lacks of catalytic activities towards ORR and is not efficient to facilitate electron transfer.[231] Deliberate doping of graphene with alien atoms (especially B and N) can transform it to an effective metal-free electrocatalyst for ORR. Electrocatatlytic ORR process, depending on the catalyst surface chemistry, often involves complex multiple steps and various

adsorbed intermediates. As for the ideal four-electron pathway, oxygen is firstly chemisorbed on the catalyst surface followed by reducing into OH^-. B, N and P dopants promote adsorption of oxygen and O-O bond cleavage because of charge polarization of heteroatom-C bond.[232-236] The catalytic ability of S- or Se-doped graphene is originated from the creation of spin density due to orbital mismatch between these heteroatoms and C. [53, 82] In some cases, charge polarization and spin density increase may simultaneous contribute (e.g., for N-doped graphene).[41, 80, 237, 238]

The wrinkles and surface tension induced by large-sized dopants also enhance ORR kinetics by promoting charge transfer.[239, 240] Binary doping of impurity atoms into graphene (e.g. B-N,[69, 201, 236] P-N,[201] N-S/Se[45, 80, 95]) reveals the synergistic effects from different co-dopants on ORR parameters (e.g. onset potential, current density and electron transfer number). More thorough discussion on B, N, P, S and Se doped graphene or other carbon materials for ORR applications can be found in several excellent review articles.[29, 241, 242]

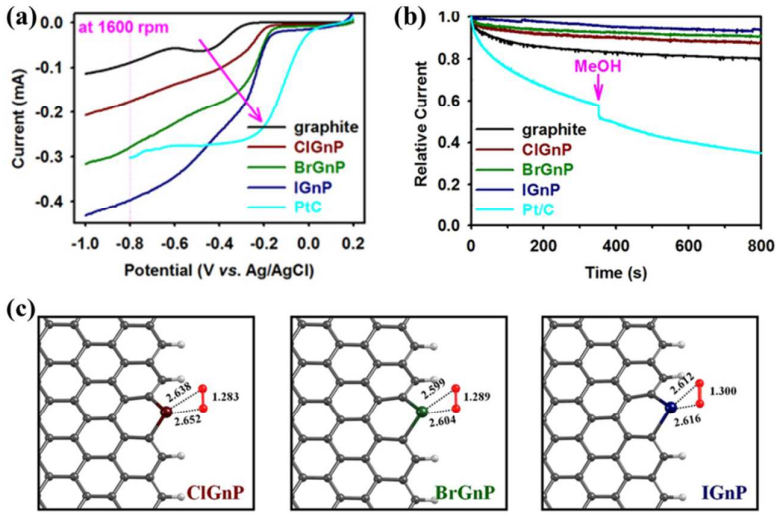

Fig. 20 (a) Linear sweep voltammograms (LSV) at a rotation rate of 1600 rpm and a scan rate of 10 mV/s, showing a gradual increase in current and a positive shift in the onset potential along the order of the pristine graphite, ClGnP, BrGnP, IGnP, Pt/C (pink arrow). (b) The current-time (j–t) chronoamperometric responses for ORR at the pristine graphite, XGnPs, and commercial Pt/C electrocatalysts in an O_2-saturated 0.1 M aq. KOH solution at -0.40 V vs. Ag/AgCl and 3.0 M methanol or carbon monoxide (CO, 10 ppm/min) were added at around 360 s. (c) The optimized O_2 adsorption geometries onto XGnPs, in which halogen covalently linked to two sp^2 carbons. The

O-O bond length and the shortest C-O bond are shown in angstroms. Adapted with permission from ref. 51. Copyright (2013) Nature Publishing Group.

Halogen-doped graphene for ORR is much less explored albeit their interesting physicochemical and electrical properties. Jeon *et al.* synthesized a series of halogenated graphene nanoplates (XGnPs, X=Cl, Br, or I) by simple ball milling technique and investigated their electrocatalytic performance towards ORR.[51] Halogen atoms are selectively doped at the edge of GnP with doping level of 5.89 at% Cl, 2.78 at% Br and 0.95 at% I, respectively. As shown in Fig. 20a, the ORR performance of XGnPs increases in the order of IGnP > BrGnP > ClGnP, which is contrary to the order of the dopant's electronegativity: Cl (3.16) > Br (2.96) > I (2.66). The excellent performance of IGnP (~3.9 electrons) is close to the ideal four-electron process. DFT calculations show that substitution bonding at zigzag edge (e.g. $-Cl^{+}-$, $-Br^{+}-$, $-I^{+}-$) are favorable for O_2 adsorption and O-O bond weakening as evidenced by the increased bond length (Fig. 20c). This is also attributable to the charge transfer between halogen and O_2, the efficiency of which follows the order of Cl < Br < I. In addition to the enhanced catalytic activity, heteroatom doping may also improve long term stability, selectivity, tolerance to methanol and CO, and electrochemical window (Fig. 20b). Therefore, doped graphene materials are promising to replace the currently used precious metal catalysts (e.g., Pt). Yao *et al.* reported the excellent ORR performance of I-doped graphene synthesized by simple thermal annealing, which exhibited comparable onset potential but higher current density as compared with Pt/C electrode.[85] I_3^- induced charge polarization is believed to play a critical role. The ORR performance of doped graphene could be further enhanced by hybridizing it with other catalysts (e.g., Fe_3O_4 or Co_3O_4[103, 243]).

Despite the tremendous progress in the use of doped-graphene materials as metal-free catalyst, the mechanisms of doping induced ORR enhancement is still not completely understood. In fact, some theoretical and experimental results are contradicting to each other,[65, 70, 71, 74, 244-246] resulting from the large heterogeneity in the properties and structures of doped-graphene materials obtained from the current synthesis methods. The possible existence of a trace amount of metal species introduced by the synthesis procedure may also affect ORR performance and hence lead to misinterpretation.[58, 247, 248] Understanding of binary and ternary doped graphene materials is even

more challenging.

Doped graphene materials have also been employed as anode materials, especially in direct methanol fuel cells (DMFC). Heteroatom doped graphene with uniform and dense decoration of precious metal catalysts can improve the catalytic activity and durability of the electrode.[249] Wang *et al.* used S-doped graphene/ Pt nanowire composite (S-doped graphene/PtNW) as both cathode for ORR and anode for methanol oxidation reaction (MOR) (Fig. 21a and b).[81] Towards ORR, it exhibits a higher current density and a lower reduction potential than the state-of-the-art Pt/C catalyst (Fig. 21c). In the case of MOR, the S-doped graphene/PtNW electrode gives ~3 times higher peak current density in comparison with Pt/C electrode (Fig. 21d). N-doped graphene-CNT hybrid with coated PtRu has also been used as DMFC anode, which offers a higher (> 2 times) power density than the commercial PtRu/C catalyst.[250] N dopants facilitate PtRu immobilization, rendering a better stability in MOR. Outstanding MOR electrocatalytic performance has also been observed for Pt- and PtAu-modified N-doped graphene materials.[251]

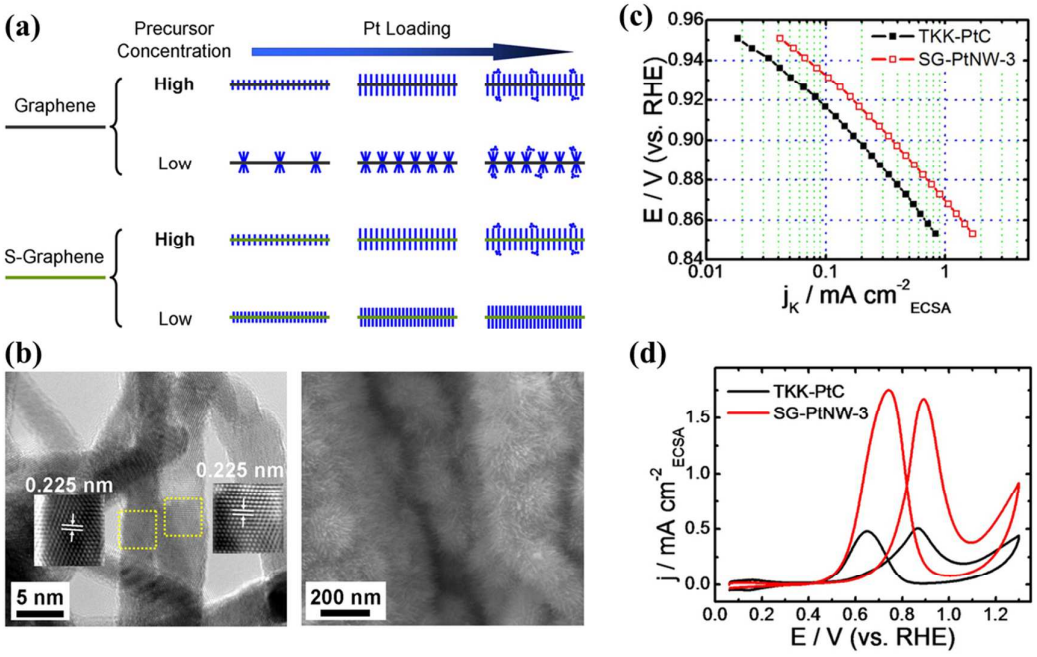

Fig. 21 (a) Schematic illustration of the nanostructural evolution of Pt nanowire arrays grown on graphene and S-doped graphene supports. (b) SEM and high resolution TEM images of S-doped graphene/PtNW catalyst. (c) Specific kinetic current densities (j_k) of S-doped graphene/PtNW and Pt/C catalysts for ORR at different potentials. (d) Specific current densities of S-doped

graphene/PtNW and Pt/C catalysts toward MOR. Adapted with permission from ref. 81. Copyright (2013) Nature Publishing Group.

4.4 Solar cells

4.4.1 Dye sensitized solar cells (DSSCs)

DSSCs are intensively researched photovoltaic devices to deal with the increasing global energy demand and environmental challenges. The counter electrode in DSSC should be highly catalytic to ensure rapid triiodide reduction and low overpotential. Since oxygen functional groups on graphene can promote reduction of I_3^- to I^-, it has been demonstrated that DSSC device with a rGO-based counter electrode (with optimized C/O ratio) exhibits a comparable power conversion efficiency (PCE) of 4.99% to that of expensive Pt counter electrode (5.48%).[252] Xu *et al.* fabricated a counter electrode using layer-by-layer composition of GO and PDDA (a cationic polymer) followed by electrochemical reduction (ER).[253] DSSC using PDDA@ERGO as the counter electrode and heteroleptic Ru complex C106TBA as the sensitizer reaches a high PCE of 9.5%. The excellent catalytic performance can be attributed to the synergistic effect of oxygen functional groups on ERGO and positively charged N groups in PDDA. Furthermore, such counter electrode exhibited excellent PCE retention (82% even after 1000 h of light soaking with full solar intensity of 1000 W m^{-2}).

Counter electrode with an optimal balance between conductivity and electrocatalytic activity is crucial. B and N doped graphene materials are not only highly catalytic to triiodide reduction but also generally more conductive to rGO. Dai's group demonstrated a DSSC equipped with a N-doped graphene (7.6 at%) foam (NGF) counter electrode which offered a PCE of 7.07% comparable to that of Pt electrode.[254] The NGF electrode exhibited a lower charge transfer resistance (R_{ct} = 5.6 Ω) than that of Pt electrode (8.8 Ω), indicating its superior catalytic activity towards I_3^-/I^- redox couple. The high porosity, good hydrophilicity and large surface of NGFs led to higher short circuit current (J_{sc} = 15.84 mA cm^{-2}), open circuit voltage (V_{oc} = 0.77V) and fill factor (FF = 0.58) than that of rGO foam, N-doped graphene film and rGO film. Cui's group showed that the electrocatalytic activity of N-doped rGO was positively scaled with the doping level.[255] Nitrogen bonding configuration is also important to determine the catalytic properties of N-doped graphene. Compared with pyrrolic N, pyridinic and graphitic N have better catalytic

activity and decreased adsorption energy toward I^-.[73]

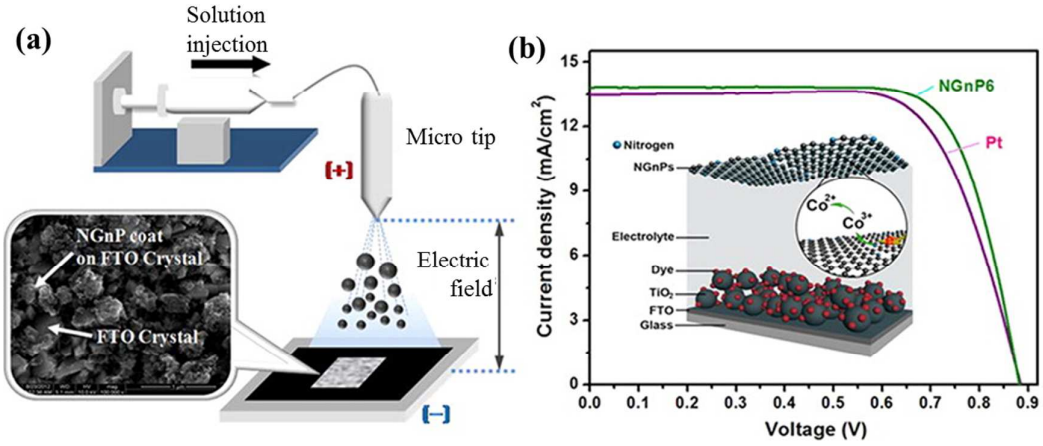

Fig. 22 (a) Schematic representation of an e-spray setup and the SEM image of NGnP coat on FTO crystal. (b) I–V characteristics of the DSSCs with Pt and NGnP CEs under one sun illumination (AM 1.5G). Inset is the schematic illustration of DSSC with an NG counter electrode and $Co(bpy)_3^{3+/2+}$ redox reduction on the surface of NGnPs. Adapted with permission from ref. 256. Copyright (2013) American Chemical Society.

Using a novel redox couple $Co(bpy)_3^{3+/2+}$ and a counter electrode fabricated by electrostatically spraying N-doped graphene nanoplatelets (NGnPs, 2.79 at%) on FTO/glass substrate, Kim *et al.* demonstrated a high-performance DSSC (PCE = 9.05%, J_{sc} = 13.83 mA cm^{-2}, FF = 74.2%) superior to the DSSC equipped with Pt counter electrode (PCE = 8.43%, J_{sc} = 13.48 mA cm^{-2}, FF = 70.6%) (Fig. 22).[256] The lower R_{ct} of NGnP electrode (1.73 Ω cm^{-2}) than that of Pt electrode (3.15Ω cm^{-2}) suggests the higher catalytic activity of NGnP. The counter electrode based on NGnPs prepared by ball milling method also significantly outperforms Pt electrode.[49] F-doped graphene is also electrocatalytic to I_3^-/I^-. Das *et al.* reported the enhanced electrocatalytic activity of graphene towards I_3^-/I^- after CF_4-plasma treatment, because of created catalytically active edges and F-doping enhanced interfacial electron-transfer. [257] It has also been shown that B-doped graphene can serve as the back electrode with desired Ohmic contact to improve hole-collection ability and photovoltaic efficiency of quantum-dot sensitized solar cells.[57]

4.4.2 Heterojunction solar cells

Like Si, heteroatom doping can endow graphene with n- or p-type semiconducting behavior.

Hence doped-graphene materials can be used for p-n junction solar cells. For example, highly transparent B-doped graphene can be used as p-type electrode in solar cells. Li *et al.* developed a solar cell by interfacing B-doped graphene with n-type Si.[32] Under 1 sun illumination, a V_{oc} of 0.53 V and J_{sc} of 18.8 mA cm^{-2} were obtained, higher than that of pristine grahpene/Si solar cell (0.33V and 15.8 $mAcm^{-2}$). Additional nitric acid fume treatment of B-doped graphene further enhanced the solar cell performance, because additional p-doping by nitric ions increased the electrical conductivity and reduced R_{ct}.[258] In similar mechanism, covalent and ionic Cl doping increases the PCE of a heterojunction solar cell from 5.52% to 8.94%.

Organic solar cells (OSCs) are photovoltaic devices possible with high flexibility, scalable fabrication process and low manufacturing cost. Bulk heterojunctions (BHJs) produced by phase-separated blending of electron donor and acceptor materials is most commonly used in OSC devices. Heteroatom doped graphene sheets can be used to improve conductivity, charge transfer, thermal and chemical stability of the active layer in BHJ-OSC. Jun *et al.* incorporated N-doped rGO (~8 at%) to the active layer of BHJ-OSC and found a large increase of J_{sc} and PCE in comparison with the device without graphene additives or with addition of undoped rGO (Fig. 23a and b).[259] N-doping induces an increase of work function (~0.4 eV), which in turn reduces R_{ct} between active polymer and grahene (Fig. 23c). The maximum PCE of ~4.39% with J_{sc} of ~14.86 mA cm^{-2} was obtained with 0.5 wt% addition of N-doped rGO. Overloading causes agglomeration of graphene sheets and parasitic paths for current leakage.

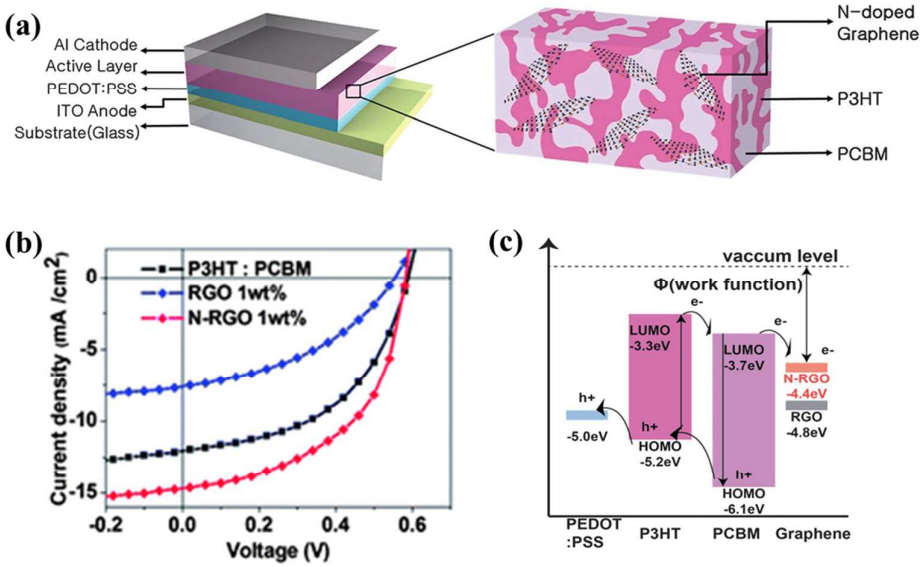

Fig. 23 (a) Schematic of the BHJ solar cell using the N-doped graphene/P3HT : PCBM active layer. (b) I–V characteristics of BHJ solar cell devices. (c) Energy-level diagram of a rGO and N-doped RGO/P3HT : PCBM OPV showing the charge generation and transfer between the two organic components to the electrodes. Adapted with permission from ref. 259. Copyright (2013) Royal Society of Chemistry.

4.5 Sensors

4.5.1 Electrochemical sensors

The performance of electrochemical sensors can be improved by the use of doped graphene materials because the electrochemically active sites introduced by heteroatom doping are able to facilitate charge transfer, adsorption and activation of analytes, and anchoring of functional moieties or molecules (e.g., analyte-specific enzymes). The intrinsic catalytic activity of doped graphene towards the analytes may eliminate the need of recognition elements or mediators (e.g., antibodies or enzymes), rendering the sensors with lower cost and higher stability.

Hydrogen peroxide (H_2O_2), which is an important signaling molecule to cells and byproduct of many biological processes, can be directly reduced by heteroatom doped graphene. Shao *et al.* reported an enzyme-free H_2O_2 sensor based on N-doped graphene electrode.[260] The sensor gave high sensitivity and a wide linear detection range (10^{-5} - 2.8 mM) because nitrogen-induced charge delocalization weakens the O-O bond of H_2O_2 and the electron-donating ability of N-dopants is advantageous for the reduction reaction.

A N-doped graphene (4.5 at%) based H_2O_2 sensor with a wide linear range (0.5 μM – 1.2 mM), low detection limit (0.05 μM), more positive onset reduction potential, higher reduction current density was developed by Wu *et al.*[87] The improved performance is due to the narrowed (50% reduction) HUMO-LUMO gap (hence higher chemical reactivity) after N-doping. Taking the advantages of the high sensitivity and specificity (against interference from other ROS species) of N-doped graphene, the authors also demonstrated the detection of triggered release of H_2O_2 from live cells. Similarly, Yang *et al.* reported an microwave-synthesized B,N co-doped graphene sensor for highly sensitive detection of H_2O_2 and its dynamic release from leukemia cells.[261] The co-doped graphene outperformed (linear range: 0.5 μM to 5 mM, detection limit: 0.05 μM) the graphene sensor with single dopant only (B or N) because the charge polarization induced by B

and N co-doping leads to better catalytic activity.

As the enzymatic catalysis of glucose is accompanied by production of H_2O_2, N-doped graphene is also promising for glucose sensing by compositing with glucose oxidase (GOD). Wang *et al.* reported an amperometric sensor based on GOD/N-doped graphene electrode, with a linear detection range of 0.1 - 1.1 mM and detection limit of 0.01 mM.[262] Owing to the high density of electronic states and active surface chemistry, N-doped graphene facilitates electron transfer from the catalytic center of GOD to the electrode surface.

N-doped grahene prepared by annealing GO with melamine was used to simultaneously and differentially detect ascorbic acid (AA), dopamine (DA) and uric acid (UA) with high sensitivity (detection limits of 2.2 μM, 0.25 μM, and 0.045 μM, respectively).[263] The high sensitivity is ensured by the strong hydrogen bonding and/or π-π interaction between N-dopants and the target molecules. Li *et al.* found that pyrrolic N is most reactive to these molecules.[264] N-doped graphene has also been used to electrochemically detect Bispheol A, a widely used industrial raw material, with a detection limit as low as 5 nM. [265]

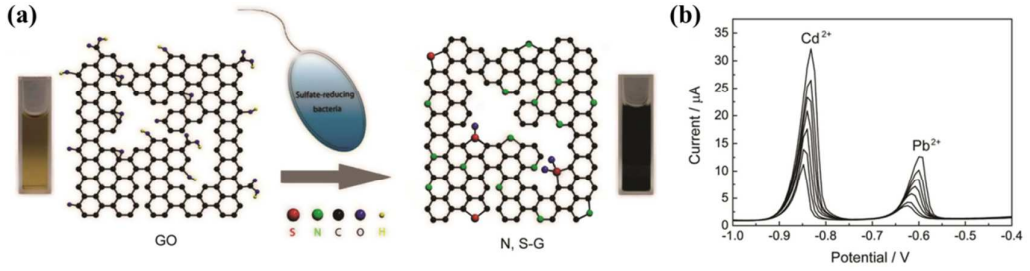

Fig. 24 (a) Schematic illustration of the formation of N,S co-doped graphene by one-pot microbial reduction process. (b) Differential pulse anodic stripping voltammetry of simultaneous analysis of $Pb^{2+}$and Cd^{2+} with concentrations of 30, 24, 18, 15, 12 and 9 μg L^{-1}, respectively. Adapted with permission from ref. 266. Copyright (2013) Nature Publishing Group.

Guo *et al.* synthesized N,S co-doped graphene (6.11 at% N dominated by pyridinic N, 1.1 at% S dominated by sulfide bonds) by reducing GO using sulfate-reducing bacteria (Fig. 24).[266] It was able to simultaneously detect Pb^{2+} (detection limit of 0.018 μg L^{-1}) and Cd^{2+} (detection limit of 0.016 μg L^{-1}), with a linear range of 9 - 30 μg L^{-1}. As compared with single-species doping (N or S alone), N,S co-doping significantly improved the electrocatalytic activity towards Cd^{2+} (> 90%) and Pb^{2+} (>20%) because of the synergistic effects between the dual dopants.

4.5.2 Electronic sensors

Graphene materials have been used as the sensing element for electronic detection of various targets taking advantages of its high carrier density and mobility, tunable electronic properties of graphene by electrostatic gating or charge transfer, and exposure of all the atoms to the sensing environment.[19, 267, 268] Heretoatom doping, which can transform graphene from semi-metal to semiconductor (with p or n-type characteristics), is advantageous for electronic detection based on filed-effect.[8] Kwon *et al.* demonstrated a field-effect transistor (FET) based on N-doped graphene for ultra-sensitive detection of vascular endothelial growth factor (VEGF) with a detection limit as low as 100 fM (Fig. 25).[39] Such N-doped graphene (n-type) was conjugated with anti-VEGF RNA aptamer for specific recognition of VEGF binding. Upon binding of positively charged VEGF molecules, an increase of source-drain current was resulted in a concentration dependent manner.

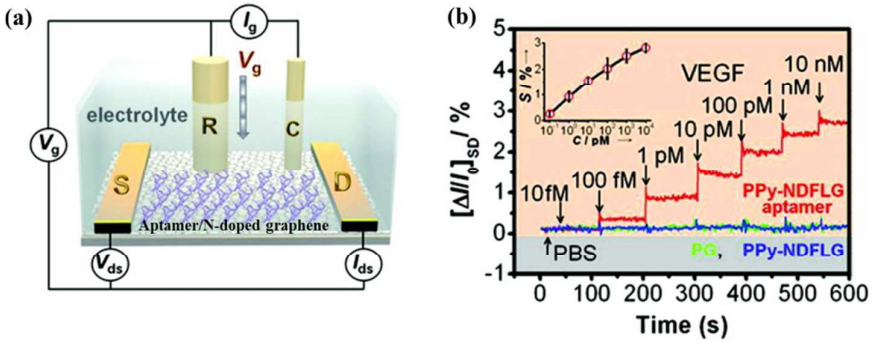

Fig. 25 (a) Schematic diagram of a liquid-ion gated FET using aptamer-conjugated N-doped graphene (Ag/AgCl reference electrode, R; platinum counter electrode, C; source and drain electrodes, S and D). (b) Real-time responses and a calibration curve (S in the inset indicates $\Delta I/I_0$) of aptasensor with various vascular endothelial growth factor concentrations. Adapted with permission from ref. 39. Copyright (2012) American Chemical Society.

Heteroatom doping can create active sites for strong adsorption of gas molecules, which, in turn, leads to dramatic change of graphene conductance. It has been theoretically proven that various electronic sensors can be developed for gas sensing. Zhang *et al.* suggested that B-doped graphene can be used for sensitive detection of NO_2.[269] Dai *et al.* showed that NO and NO_2 can be electrically detected by B or S-doped graphene devices.[184] Graphene with metal (e.g., Fe, Co) or Si dopants could be used for H_2S sensing.[270] However, for practical gas sensors, the possible inference from O_2 molecules should be considered. It has been found that Si- and P-doped

graphene invite stable chemisorption of O_2, whereas B- and N-doped graphene are inert to O_2.[271] The strong chemical reactivity of Si-doped graphene with O_2 and NO_2 was also reported by Zhou *et al.*[190]

Despite proven potentials, experimental demonstrations of doped graphene for gas sensing are rare till now. Using N,Si co-doped graphene for electrical detection of NO_2 was recently presented (Fig. 26a).[272] N,Si co-doped graphene, synthesized by simply annealing GO in the presence of Si-containing IL, shows a resistance decrease while exposing to NO_2 gas (~26% reduction at 21 ppm and 8.8% at 1 ppm) (Fig. 26b). Contradictory to the expectation from the strong chemisorption of NO_2 on Si-doped graphene, [190] this sensor shows excellent reversibility. This discrepancy may be explained by the low abundant of Si dopants and the doping configurations different to the assumed in the simulation study.

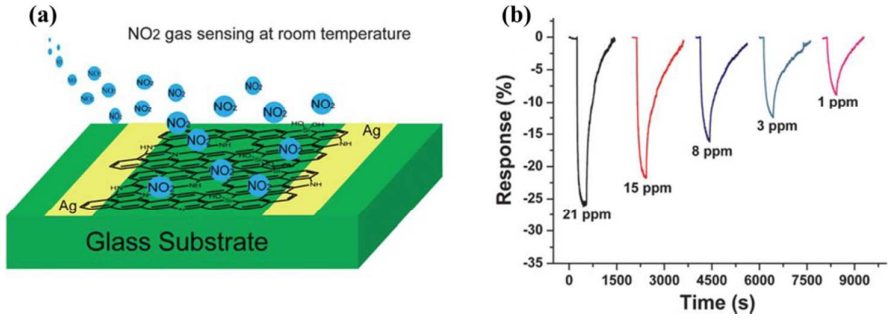

Fig. 26 (a) NO_2 sensor based on N,Si co-doped grahpene and (b) its response to NO_2 with varying concentrations. Adapted with permission from ref. 272. Copyright (2013) Royal Society of Chemistry.

4.5.3 Sensors based on surface-enhanced Raman spectroscopy (SERS)

Sensors based on SERS are able to detect the low presence and signature of the analytes utilizing electromagnetic effects induced by precious metal nanoparticles and / or charge transfer effects. It has been shown that binding of organic molecules on graphene surface can produce large SERS enhancement, which is attributed to the charge transfer between target molecules and graphene.[273] The highly polarized heteroatom-C bonds induced by doping may promote the charge transfer between the bound analytes and graphene (hence improving SERS signal). As shown by a DFT study, substitutional B-doping can increase the SERS signal of pyridine by 3 – 4 orders, accompanied with a frequency shift of ~ 30 cm^{-1}.[274] This is attributed to charge transfer between

the negatively charged N atom of pyridine and positively charged B atom on graphene. As for case of graphitic N doping (however, with a weaker response than B-doped graphene), the SERS enhancement is proposed to originate from the π electron transfer from graphene to pyridine.

Lv *et al.* experimentally demonstrated the first SERS sensor based on N-doped graphene.[275] N-doped graphene (0.25 at%, two N atoms separated by one C atom in the same A sublattice as the dominant configuration) synthesized by atmospheric-pressure CVD was used to probe Rhodamine B (RhB) molecules (Fig. 27). In comparison with pristine graphene, N-doped counterpart gave 10 times stronger signal at 1650 cm^{-1} for the fingerprints of RhB with additional vibration peaks at 1282 cm^{-1}, 1531 cm^{-1} and 1567 cm^{-1} (Fig. 27c). The charge transfer (p-doping) by RhB underlies the detection.

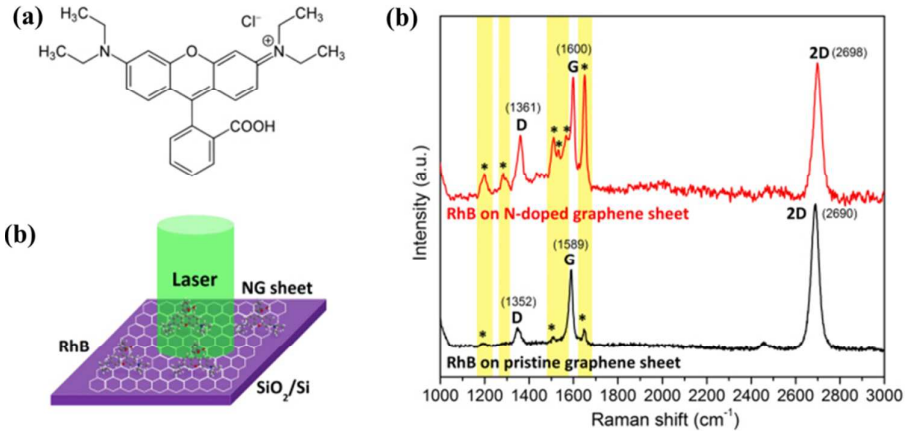

Fig. 27 Enhanced Raman scattering effect of N-doped graphene sheets for probing RhB molecules. (a) Molecular structure of RhB. (b) Schematic illustration of experimental setup. RhB molecules are anchored onto NG sheet/SiO_2/Si substrate. The laser line is 514 nm. (c) Raman signals (*) of RhB molecules. Adapted with permission from ref. 275. Copyright (2012) Nature Publishing Group.

4.6 Gas storage

Hydrogen is an ideal energy carrier with non-polluting nature and high energy density. However, its storage is currently a huge technical hurdle for transportation and practical applications. Modifying graphene materials with metal nanoparticles (e.g. alkali and alkaline earth metals) can improve the gravimetric storage capacity *via* polarization-induced interaction between metal and hydrogen atoms.[276] However, decorated nanoparticles suffer from aggregation and poor stability.

Heteroatom doping can assist nanoparticle dispersion and high coverage on graphene, as well as H_2 adsorption. Parambhath *et al.* synthesized pyrrolic-N dominant graphene (7 at%) for H_2 storage.[277] In comparison with undoped graphene, it increased H_2 storage capabilities by 66% (0.88 wt%) at 25 °C and 2 MPa. A further 124% enhancement was achieved with additional decoration of Pd nanoparticles. The highly dispersed and strongly bonded Pd nanoparticles promote H_2 dissociation and the resulting hydrogen atom migration to the underneath of N-doped graphene. It has been theoretically predicted that H_2 absorption on N-doped graphene can be further strengthened by adsorbed Li atoms.[278, 279]

B doping-induced graphene polarization and electron deficiency is also favorable for hydrogen adsorption, which is even more effective than graphitic-N doping.[118, 280] Theoretical calculations show a high H_2 storage capacity (8.38 wt%) of Ca-decorated B-doped (12 at%) graphene.[281] And the desirable interaction between H_2 and B,Ca-decorated graphene makes H_2 storage possible at room temperature and ambient pressure.

Developing techniques to capture greenhouse gases (e.g., CO_2) is critical to deal with global warming. Kim and co-workers reported a high gravimetric CO_2 storage capacity (2.7 mmol g^{-1}, at 298 K and 1 atm) of N-doped graphene, which is comparable to that of PANI-graphene composite at high pressure.[282] The superior performance is attributable to the strong interaction between N-dopants and CO_2 molecules. It is also demonstrated that these N-doped graphene materials possess high recycling stability and selectivity over N_2, CH_4 and H_2. Heteroatom doped graphene could be used to capture other gases considering its high binding affinity with other gas molecules (e.g., NO, NO_2, SO_2).[184]

5 Summary and perspectives

As discussed in this article, heteroatom doping can endow graphene with various new electromagnetic, physicochemical, optical, and structural properties, depending on the dopants and doping configurations. This greatly extends the arsenal of graphene materials and their potentials for a spectrum of applications. Different approaches have been developed for heteroatom doping. Doping type, level and configurations (hence the properties of obtained materials) are critically determined by chosen precursors, starting graphene material, reaction time, temperature, etc.

Despite the tremendous progress made thus far, it is, however, still a current challenge to precisely control heteroatom doping. Based on both experimental and theoretical studies, we have comparably discussed the distinct effects induced by specific dopants, different bonding configurations of a given dopant, and synergistic actions between co-dopants. But the current understanding on the properties of doped graphene materials is still far from complete and sometimes even contradictory because of the large and uncontrolled heterogeneity of the materials obtained from the current synthesis approaches.

The emerging applications of doped graphene materials for energy storage, energy conversion, sensors, and gas storage have been surveyed here. We envision that better understanding on doping mechanisms and doping properties based on both theoretical and experimental investigations, further development of controllable synthesis methods, and incorporation of new dopants will greatly extend the application scope of doped graphene materials. As different dopants, doping configurations and their relative ratios, and compositions of co-dopants confer graphene with distinct properties, selection and engineering of these parameters should be application-specific. For example, multi-dopants with the optimal balance, which can simultaneously enhance charge polarization, spin density, and conductivity, are desired for ORR.

When graphene transform from its native 2D structure to 1D (nanoribbons) or 0D (graphene quantum dots - GQD), dramatically altered or new properties arise due to quantum confinement and edge effects. Although not discussed here, we speculate that heteroatom doping on 1D and 0D graphene materials will open up new horizons in graphene research and applications. For example, it has been shown that the fluorescent properties of GQDs can be tailored by heteroatom doping for novel bio-imaging or optical sensing applications.[283-286]

Graphene research will continue to thrive because of the new opportunities provided by heteroatom doping. This article aims to provide useful clues for developing new and controllable synthesis methods and better understanding of the properties of doped graphene materials. We also hope that it will inspire more exciting applications of this growing family of nanomaterials.

Acknowledgement

We thank the support from Ministry of Education of Singapore under an AcRF Tier 2 grant (MOE2011-T2-2-010, MOE2012-T2-2-049), the Agency for Science, Technology and Research (A*STAR) under a SERC Grant (102 170 0142), and NNSF of China (61328401).

References

1. A. K. Geim and K. S. Novoselov, *Nature Materials*, 2007, **6**, 183-191.
2. A. H. Castro Neto, F. Guinea, N. M. R. Peres, K. S. Novoselov and A. K. Geim, *Reviews of Modern Physics*, 2009, **81**, 109-162.
3. D. Jariwala, V. K. Sangwan, L. J. Lauhon, T. J. Marks and M. C. Hersam, *Chemical Society Reviews*, 2013, **42**, 2824-2860.
4. K. C. Yung, W. M. Wu, M. P. Pierpoint and F. V. Kusmartsev, *Contemporary Physics*, 2013, **54**, 233-251.
5. N. Mahmood, C. Z. Zhang, H. Yin and Y. L. Hou, *Journal of Materials Chemistry A*, 2014, **2**, 15-32.
6. Y. Q. Sun, Q. O. Wu and G. Q. Shi, *Energy & Environmental Science*, 2011, **4**, 1113-1132.
7. J. Zhang, F. Zhao, Z. P. Zhang, N. Chen and L. T. Qu, *Nanoscale*, 2013, **5**, 3112-3126.
8. Y. X. Liu, X. C. Dong and P. Chen, *Chem Soc Rev*, 2012, **41**, 2283-2307.
9. L. Y. Feng, L. Wu and X. G. Qu, *Advanced Materials*, 2013, **25**, 168-186.
10. K. Yang, Y. J. Li, X. F. Tan, R. Peng and Z. Liu, *Small*, 2013, **9**, 1492-1503.
11. D. Zhan, J. X. Yan, L. F. Lai, Z. H. Ni, L. Liu and Z. X. Shen, *Advanced Materials*, 2012, **24**, 4055-4069.
12. W. L. Wei and X. G. Qu, *Small*, 2012, **8**, 2138-2151.
13. Y. W. Zhu, S. Murali, W. W. Cai, X. S. Li, J. W. Suk, J. R. Potts and R. S. Ruoff, *Adv. Mater.*, 2010, **22**, 3906-3924.
14. X. T. Zheng, A. Than, A. Ananthanaraya, D. H. Kim and P. Chen, *Acs Nano*, 2013, **7**, 6278-6286.
15. J. H. Shen, Y. H. Zhu, X. L. Yang and C. Z. Li, *Chemical Communications*, 2012, **48**, 3686-3699.
16. L. L. Li, G. H. Wu, G. H. Yang, J. Peng, J. W. Zhao and J. J. Zhu, *Nanoscale*, 2013, **5**, 4015-4039.
17. A. Ananthanarayanan, X. W. Wang, P. Routh, B. Sana, S. Lim, D. H. Kim, K. H. Lim, J. Li and P. Chen, *Adv. Funct. Mater.*, Doi: 10.1002/adfm.201303441.
18. S. Dutta and S. K. Pati, *Journal of Materials Chemistry*, 2010, **20**, 8207-8223.
19. X. Dong, Q. Long, J. Wang, M. B. Chan-Park, Y. Huang, W. Huang and P. Chen, *Nanoscale*, 2011, **3**, 5156-5160.
20. C. Li and G. Q. Shi, *Nanoscale*, 2012, **4**, 5549-5563.
21. X. C. Dong, H. Xu, X. W. Wang, Y. X. Huang, M. B. Chan-Park, H. Zhang, L. H. Wang, W. Huang and P. Chen, *Acs Nano*, 2012, **6**, 3206-3213.
22. Y. C. Yong, X. C. Dong, M. B. Chan-Park, H. Song and P. Chen, *Acs Nano*, 2012, **6**, 2394-2400.
23. X. C. Dong, D. L. Fu, W. J. Fang, Y. M. Shi, P. Chen and L. J. Li, *Small*, 2009, **5**, 1422-1426.

24. X. C. Dong, Q. Long, A. Wei, W. J. Zhang, L. J. Li, P. Chen and W. Huang, *Carbon*, 2012, **50**, 1517-1522.
25. V. Georgakilas, M. Otyepka, A. B. Bourlinos, V. Chandra, N. Kim, K. C. Kemp, P. Hobza, R. Zboril and K. S. Kim, *Chemical Reviews*, 2012, **112**, 6156-6214.
26. R. T. Lv and M. Terrones, *Materials Letters*, 2012, **78**, 209-218.
27. U. N. Maiti, W. J. Lee, J. M. Lee, Y. Oh, J. Y. Kim, J. E. Kim, J. Shim, T. H. Han and S. O. Kim, *Adv. Mater.*, 2014, **26**, 40-67.
28. X. K. Kong, C. L. Chen and Q. W. Chen, *Chem Soc Rev*, 2014, **43**, 2841-2857.
29. D. W. Wang and D. S. Su, *Energy & Environmental Science*, 2014, **7**, 576-591.
30. C. K. Chang, S. Kataria, C. C. Kuo, A. Ganguly, B. Y. Wang, J. Y. Hwang, K. J. Huang, W. H. Yang, S. B. Wang, C. H. Chuang, M. Chen, C. I. Huang, W. F. Pong, K. J. Song, S. J. Chang, J. H. Guo, Y. Tai, M. Tsujimoto, S. Isoda, C. W. Chen, L. C. Chen and K. H. Chen, *Acs Nano*, 2013, **7**, 1333-1341.
31. T. R. Wu, H. L. Shen, L. Sun, B. Cheng, B. Liu and J. C. Shen, *New Journal of Chemistry*, 2012, **36**, 1385-1391.
32. X. Li, L. L. Fan, Z. Li, K. L. Wang, M. L. Zhong, J. Q. Wei, D. H. Wu and H. W. Zhu, *Advanced Energy Materials*, 2012, **2**, 425-429.
33. L. Ci, L. Song, C. H. Jin, D. Jariwala, D. X. Wu, Y. J. Li, A. Srivastava, Z. F. Wang, K. Storr, L. Balicas, F. Liu and P. M. Ajayan, *Nat Mater*, 2010, **9**, 430-435.
34. G. Bepete, D. Voiry, M. Chhowalla, Z. Chiguvare and N. J. Coville, *Nanoscale*, 2013, **5**, 6552-6557.
35. Y. H. Xue, D. S. Yu, L. M. Dai, R. G. Wang, D. Q. Li, A. Roy, F. Lu, H. Chen, Y. Liu and J. Qu, *Physical Chemistry Chemical Physics*, 2013, **15**, 12220-12226.
36. H. Wang, Y. Zhou, D. Wu, L. Liao, S. L. Zhao, H. L. Peng and Z. F. Liu, *Small*, 2013, **9**, 1316-1320.
37. A. L. M. Reddy, A. Srivastava, S. R. Gowda, H. Gullapalli, M. Dubey and P. M. Ajayan, *Acs Nano*, 2010, **4**, 6337-6342.
38. Z. Jin, J. Yao, C. Kittrell and J. M. Tour, *Acs Nano*, 2011, **5**, 4112-4117.
39. O. S. Kwon, S. J. Park, J. Y. Hong, A. R. Han, J. S. Lee, J. S. Lee, J. H. Oh and J. Jang, *Acs Nano*, 2012, **6**, 1486-1493.
40. Z. Z. Sun, Z. Yan, J. Yao, E. Beitler, Y. Zhu and J. M. Tour, *Nature*, 2010, **468**, 549-552.
41. Y. W. Zhang, J. Ge, L. Wang, D. H. Wang, F. Ding, X. M. Tao and W. Chen, *Scientific Reports*, 2013, **3**.
42. D. C. Wei, Y. Q. Liu, Y. Wang, H. L. Zhang, L. P. Huang and G. Yu, *Nano Letters*, 2009, **9**, 1752-1758.
43. L. T. Qu, Y. Liu, J. B. Baek and L. M. Dai, *Acs Nano*, 2010, **4**, 1321-1326.
44. H. Gao, Z. Liu, L. Song, W. H. Guo, W. Gao, L. J. Ci, A. Rao, W. J. Quan, R. Vajtai and P. M. Ajayan, *Nanotechnology*, 2012, **23**.
45. J. X. Xu, G. F. Dong, C. H. Jin, M. H. Huang and L. H. Guan, *Chemsuschem*, 2013, **6**, 493-499.
46. G. Kalita, K. Wakita, M. Takahashi and M. Umeno, *Journal of Materials Chemistry*, 2011, **21**, 15209-15213.
47. I. Y. Jeon, Y. R. Shin, G. J. Sohn, H. J. Choi, S. Y. Bae, J. Mahmood, S. M. Jung, J. M. Seo, M. J. Kim, D. W. Chang, L. M. Dai and J. B. Baek, *P Natl Acad Sci USA*, 2012, **109**, 5588-5593.
48. L. Yan, M. M. Lin, C. Zeng, Z. Chen, S. Zhang, X. M. Zhao, A. G. Wu, Y. P. Wang, L. M. Dai, J. Qu, M. M. Guo and Y. Liu, *J Mater Chem*, 2012, **22**, 8367-8371.
49. I. Y. Jeon, H. J. Choi, M. J. Ju, I. T. Choi, K. Lim, J. Ko, H. K. Kim, J. C. Kim, J. J. Lee, D. Shin, S. M.

Jung, J. M. Seo, M. J. Kim, N. Park, L. Dai and J. B. Baek, *Scientific Reports*, 2013, **3**.

50. K. Brenner and R. Murali, *Applied Physics Letters*, 2011, **98**.
51. I. Y. Jeon, H. J. Choi, M. Choi, J. M. Seo, S. M. Jung, M. J. Kim, S. Zhang, L. P. Zhang, Z. H. Xia, L. M. Dai, N. Park and J. B. Baek, *Scientific Reports*, 2013, **3**.
52. I. Y. Jeon, H. J. Choi, S. M. Jung, J. M. Seo, M. J. Kim, L. M. Dai and J. B. Baek, *J Am Chem Soc*, 2013, **135**, 1386-1393.
53. I. Y. Jeon, S. Zhang, L. P. Zhang, H. J. Choi, J. M. Seo, Z. H. Xia, L. M. Dai and J. B. Baek, *Advanced Materials*, 2013, **25**, 6138-6145.
54. X. J. Lu, J. J. Wu, T. Q. Lin, D. Y. Wan, F. Q. Huang, X. M. Xie and M. H. Jiang, *Journal of Materials Chemistry*, 2011, **21**, 10685-10689.
55. D. H. Deng, X. L. Pan, L. A. Yu, Y. Cui, Y. P. Jiang, J. Qi, W. X. Li, Q. A. Fu, X. C. Ma, Q. K. Xue, G. Q. Sun and X. H. Bao, *Chemistry of Materials*, 2011, **23**, 1188-1193.
56. D. Geng, Y. Hu, Y. Li, R. Li and X. Sun, *Electrochemistry Communications*, 2012, **22**, 65-68.
57. T. Q. Lin, F. Q. Huang, J. Liang and Y. X. Wang, *Energy & Environmental Science*, 2011, **4**, 862-865.
58. H. L. Peng, Z. Y. Mo, S. J. Liao, H. G. Liang, L. J. Yang, F. Luo, H. Y. Song, Y. L. Zhong and B. Q. Zhang, *Scientific Reports*, 2013, **3**.
59. Z. S. Wu, W. C. Ren, L. Xu, F. Li and H. M. Cheng, *Acs Nano*, 2011, **5**, 5463-5471.
60. Z. C. Zuo, Z. Q. Jiang and A. Manthiram, *Journal of Materials Chemistry A*, 2013, **1**, 13476-13483.
61. X. L. Li, H. L. Wang, J. T. Robinson, H. Sanchez, G. Diankov and H. J. Dai, *Journal of the American Chemical Society*, 2009, **131**, 15939-15944.
62. L. S. Zhang, X. Q. Liang, W. G. Song and Z. Y. Wu, *Physical Chemistry Chemical Physics*, 2010, **12**, 12055-12059.
63. G. H. Jun, S. H. Jin, B. Lee, B. H. Kim, W. S. Chae, S. H. Hong and S. Jeon, *Energy & Environmental Science*, 2013, **6**, 3000-3006.
64. B. Xiong, Y. K. Zhou, Y. Y. Zhao, J. Wang, X. Chen, R. O'Hayre and Z. P. Shao, *Carbon*, 2013, **52**, 181-192.
65. D. S. Geng, Y. Chen, Y. G. Chen, Y. L. Li, R. Y. Li, X. L. Sun, S. Y. Ye and S. Knights, *Energy & Environmental Science*, 2011, **4**, 760-764.
66. E. Yoo, J. Nakamura and H. S. Zhou, *Energy & Environmental Science*, 2012, **5**, 6928-6932.
67. T. V. Khai, H. G. Na, D. S. Kwak, Y. J. Kwon, H. Ham, K. B. Shim and H. W. Kim, *Journal of Materials Chemistry*, 2012, **22**, 17992-18003.
68. H. B. Wang, C. J. Zhang, Z. H. Liu, L. Wang, P. X. Han, H. X. Xu, K. J. Zhang, S. M. Dong, J. H. Yao and G. L. Cui, *Journal of Materials Chemistry*, 2011, **21**, 5430-5434.
69. S. Y. Wang, L. P. Zhang, Z. H. Xia, A. Roy, D. W. Chang, J. B. Baek and L. M. Dai, *Angewandte Chemie-International Edition*, 2012, **51**, 4209-4212.
70. L. F. Lai, J. R. Potts, D. Zhan, L. Wang, C. K. Poh, C. H. Tang, H. Gong, Z. X. Shen, L. Y. Jianyi and R. S. Ruoff, *Energy & Environmental Science*, 2012, **5**, 7936-7942.
71. Z. H. Sheng, L. Shao, J. J. Chen, W. J. Bao, F. B. Wang and X. H. Xia, *Acs Nano*, 2011, **5**, 4350-4358.
72. Z. Y. Lin, G. H. Waller, Y. Liu, M. L. Liu and C. P. Wong, *Carbon*, 2013, **53**, 130-136.
73. S. C. Hou, X. Cai, H. W. Wu, X. Yu, M. Peng, K. Yan and D. C. Zou, *Energy & Environmental Science*, 2013, **6**, 3356-3362.

74. C. H. Choi, M. W. Chung, S. H. Park and S. I. Woo, *Rsc Advances*, 2013, **3**, 4246-4253.
75. J. Y. Liu, H. Y. Chang, Q. D. Truong and Y. C. Ling, *Journal of Materials Chemistry C*, 2013, **1**, 1713-1716.
76. R. Li, Z. Wei, X. Gou and W. Xu, *RSC Advances*, 2013, **3**, 9978-9984.
77. S. B. Yang, L. J. Zhi, K. Tang, X. L. Feng, J. Maier and K. Mullen, *Advanced Functional Materials*, 2012, **22**, 3634-3640.
78. H. L. Poh, P. Simek, Z. Sofer and M. Pumera, *Acs Nano*, 2013, **7**, 5262-5272.
79. M. Seredych, J. C. Idrobo and T. J. Bandosz, *Journal of Materials Chemistry A*, 2013, **1**, 7059-7067.
80. C. H. Choi, M. W. Chung, Y. J. Jun and S. I. Woo, *Rsc Advances*, 2013, **3**, 12417-12422.
81. R. Y. Wang, D. C. Higgins, M. A. Hoque, D. Lee, F. Hassan and Z. W. Chen, *Scientific Reports*, 2013, **3**.
82. Z. Yang, Z. Yao, G. F. Li, G. Y. Fang, H. G. Nie, Z. Liu, X. M. Zhou, X. Chen and S. M. Huang, *Acs Nano*, 2012, **6**, 205-211.
83. J. Liang, Y. Jiao, M. Jaroniec and S. Z. Qiao, *Angewandte Chemie-International Edition*, 2012, **51**, 11496-11500.
84. H. L. Poh, P. Simek, Z. Sofer and M. Pumera, *Chemistry-a European Journal*, 2013, **19**, 2655-2662.
85. Z. Yao, H. G. Nie, Z. Yang, X. M. Zhou, Z. Liu and S. M. Huang, *Chemical Communications*, 2012, **48**, 1027-1029.
86. P. Wu, Z. W. Cai, Y. Gao, H. Zhang and C. X. Cai, *Chemical Communications*, 2011, **47**, 11327-11329.
87. P. Wu, Y. D. Qian, P. Du, H. Zhang and C. X. Cai, *Journal of Materials Chemistry*, 2012, **22**, 6402-6412.
88. Y. H. S. Park, J. O. Hwang, E.-S. Lee, L. B. Casabianca, W. Cai, J. R. Potts, H.-W. Ha, S. Chen, J. Oh, S. O. Kim, Y.-H. Kim, Y. Ishii and R. S. Ruoff,, *Nature communications*, 2012, **3**, 1-8.
89. D. H. Long, W. Li, L. C. Ling, J. Miyawaki, I. Mochida and S. H. Yoon, *Langmuir*, 2010, **26**, 16096-16102.
90. B. Jiang, C. Tian, L. Wang, L. Sun, C. Chen, X. Nong, Y. Qiao and H. Fu, *Applied Surface Science*, 2012, **258**, 3438-3443.
91. L. Sun, L. Wang, C. G. Tian, T. X. Tan, Y. Xie, K. Y. Shi, M. T. Li and H. G. Fu, *Rsc Advances*, 2012, **2**, 4498-4506.
92. J. W. Lee, J. M. Ko and J. D. Kim, *Electrochimica Acta*, 2012, **85**, 459-466.
93. Y. J. Zhang, K. Fugane, T. Mori, L. Niu and J. H. Ye, *Journal of Materials Chemistry*, 2012, **22**, 6575-6580.
94. Y. Z. Chang, G. Y. Han, J. P. Yuan, D. Y. Fu, F. F. Liu and S. D. A. Li, *Journal of Power Sources*, 2013, **238**, 492-500.
95. Y. Z. Su, Y. Zhang, X. D. Zhuang, S. Li, D. Q. Wu, F. Zhang and X. L. Feng, *Carbon*, 2013, **62**, 296-301.
96. R. Ballesteros-Garrido, H. G. Baldovi, M. Latorre-Sanchez, M. Alvaro and H. Garcia, *Journal of Materials Chemistry A*, 2013, **1**, 11728-11734.
97. P. W. Gong, Z. F. Wang, J. Q. Wang, H. G. Wang, Z. P. Li, Z. J. Fan, Y. Xu, X. X. Han and S. R. Yang, *Journal of Materials Chemistry*, 2012, **22**, 16950-16956.
98. H. X. Chang, J. S. Cheng, X. Q. Liu, J. F. Gao, M. J. Li, J. H. Li, X. M. Tao, F. Ding and Z. J. Zheng,

Chemistry-a European Journal, 2011, **17**, 8896-8903.

99. J. Zheng, H. T. Liu, B. Wu, C. A. Di, Y. L. Guo, T. Wu, G. Yu, Y. Q. Liu and D. B. Zhu, *Scientific Reports*, 2012, **2**.
100. H. L. Guo, P. Su, X. F. Kang and S. K. Ning, *Journal of Materials Chemistry A*, 2013, **1**, 2248-2255.
101. Z. S. Wu, A. Winter, L. Chen, Y. Sun, A. Turchanin, X. L. Feng and K. Mullen, *Advanced Materials*, 2012, **24**, 5130-5135.
102. Y. Y. Zhao, Y. K. Zhou, B. Xiong, J. Wang, X. Chen, R. O'Hayre and Z. P. Shao, *Journal of Solid State Electrochemistry*, 2013, **17**, 1089-1098.
103. Z. S. Wu, S. B. Yang, Y. Sun, K. Parvez, X. L. Feng and K. Mullen, *Journal of the American Chemical Society*, 2012, **134**, 9082-9085.
104. S. H. Yang, X. F. Song, P. Zhang and L. Gao, *Acs Applied Materials & Interfaces*, 2013, **5**, 3317-3322.
105. R. F. Nie, J. J. Shi, W. C. Du, W. S. Ning, Z. Y. Hou and F. S. Xiao, *Journal of Materials Chemistry A*, 2013, **1**, 9037-9045.
106. C. Nethravathi, C. R. Rajamathi, M. Rajamathi, U. K. Gautam, X. Wang, D. Golberg and Y. Bando, *Acs Applied Materials & Interfaces*, 2013, **5**, 2708-2714.
107. P. H. Shi, R. J. Su, F. Z. Wan, M. C. Zhu, D. X. Li and S. H. Xu, *Applied Catalysis B-Environmental*, 2012, **123**, 265-272.
108. H. M. Jeong, J. W. Lee, W. H. Shin, Y. J. Choi, H. J. Shin, J. K. Kang and J. W. Choi, *Nano letters*, 2011, **11**, 2472-2477.
109. Y. Wang, Y. Shao, D. W. Matson, J. Li and Y. Lin, *ACS Nano*, 2010, **4**, 1790-1798.
110. S. Gulbagh, D. S. Sutar, V. D. Botcha, K. N. Pavan, S. S. Talwar, R. S. Srinivasa and S. S. Major, *Nanotechnology*, 2013, **24**, 355704.
111. J. Wu, L. M. Xie, Y. G. Li, H. L. Wang, Y. J. Ouyang, J. Guo and H. J. Dai, *Journal of the American Chemical Society*, 2011, **133**, 19668-19671.
112. X. Zhang, A. Hsu, H. Wang, Y. Song, J. Kong, M. S. Dresselhaus and T. Palacios, *Acs Nano*, 2013, **7**, 7262-7270.
113. B. Li, L. Zhou, D. Wu, H. L. Peng, K. Yan, Y. Zhou and Z. F. Liu, *Acs Nano*, 2011, **5**, 5957-5961.
114. N. Li, Z. Y. Wang, K. K. Zhao, Z. J. Shi, Z. N. Gu and S. K. Xu, *Carbon*, 2010, **48**, 255-259.
115. L. S. Panchakarla, K. S. Subrahmanyam, S. K. Saha, A. Govindaraj, H. R. Krishnamurthy, U. V. Waghmare and C. N. R. Rao, *Advanced materials*, 2009, **21**, 4726-4730.
116. B. S. Shen, J. T. Chen, X. B. Yan and Q. J. Xue, *Rsc Advances*, 2012, **2**, 6761-6764.
117. P. Rani and V. K. Jindal, *Rsc Advances*, 2013, **3**, 802-812.
118. R. H. Miwa, T. B. Martins and A. Fazzio, *Nanotechnology*, 2008, **19**.
119. R. Faccio, L. Fernandez-Werner, H. Pardo, C. Goyenola, O. N. Ventura and A. W. Mombru, *Journal of Physical Chemistry C*, 2010, **114**, 18961-18971.
120. K. Z. M. Magdalena Woi´nska, and Jacek A. Majewski, *Physica Status Solidi C*, 2013, **10**, 1167-1171.
121. L. S. Panchokarla, K. S. Subrahmanyam, S. K. Saha, A. Govindaraj, H. R. Krishnamurthy, U. V. Waghmare and C. N. R. Rao, *Advanced Materials*, 2009, **21**, 4726-+.
122. B. Mortazavi and S. Ahzi, *Solid State Communications*, 2012, **152**, 1503-1507.
123. B. Zheng, P. Hermet and L. Henrard, *Acs Nano*, 2010, **4**, 4165-4173.
124. Q. Q. Zhu, J. H. Yu, W. S. Zhang, H. Z. Dong and L. F. Dong, *Journal of Renewable and*

Sustainable Energy, 2013, **5**.

125. S. Mukherjee and T. P. Kaloni, *Journal of Nanoparticle Research*, 2012, **14**.
126. A. Lherbier, X. Blase, Y. M. Niquet, F. Triozon and S. Roche, *Physical Review Letters*, 2008, **101**.
127. H. Mousavi and R. Moradian, *Solid State Sciences*, 2011, **13**, 1459-1464.
128. S. O. Guillaume, B. Zheng, J. C. Charlier and L. Henrard, *Physical Review B*, 2012, **85**.
129. D. Usachov, O. Vilkov, A. Gruneis, D. Haberer, A. Fedorov, V. K. Adamchuk, A. B. Preobrajenski, P. Dudin, A. Barinov, M. Oehzelt, C. Laubschat and D. V. Vyalikh, *Nano letters*, 2011, **11**, 5401-5407.
130. M. M. Yang, L. Zhou, J. Y. Wang, Z. F. Liu and Z. R. Liu, *Journal of Physical Chemistry C*, 2012, **116**, 844-850.
131. Z. F. Hou, X. L. Wang, T. Ikeda, K. Terakura, M. Oshima and M. Kakimoto, *Physical Review B*, 2013, **87**.
132. Z. F. Hou, X. L. Wang, T. Ikeda, K. Terakura, M. Oshima, M. Kakimoto and S. Miyata, *Physical Review B*, 2012, **85**.
133. P. Wu, P. Du, H. Zhang and C. Cai, *Physical Chemistry Chemical Physics*, 2013, **15**, 6920-6928.
134. A. Lherbier, A. R. Botello-Mendez and J. C. Charlier, *Nano letters*, 2013, **13**, 1446-1450.
135. D. Wei, Y. Liu, Y. Wang, H. Zhang, L. Huang and G. Yu, *Nano letters*, 2009, **9**, 1752-1758.
136. S. Jalili and R. Vaziri, *Molecular Physics*, 2011, **109**, 687-694.
137. T. Schiros, D. Nordlund, L. Palova, D. Prezzi, L. Y. Zhao, K. S. Kim, U. Wurstbauer, C. Gutierrez, D. Delongchamp, C. Jaye, D. Fischer, H. Ogasawara, L. G. M. Pettersson, D. R. Reichman, P. Kim, M. S. Hybertsen and A. N. Pasupathy, *Nano letters*, 2012, **12**, 4025-4031.
138. M. M. Xie, Y. J. Su, X. N. Lu, Y. Z. Zhang, Z. Yang and Y. F. Zhang, *Mater Lett*, 2013, **93**, 161-164.
139. F. Cervantes-Sodi, G. Csanyi, S. Piscanec and A. C. Ferrari, *Physical Review B*, 2008, **77**.
140. E. Velez-Fort, C. Mathieu, E. Pallecchi, M. Pigneur, M. G. Silly, R. Belkhou, M. Marangolo, A. Shukla, F. Sirotti and A. Ouerghi, *Acs Nano*, 2012, **6**, 10893-10900.
141. J. O. Hwang, J. S. Park, D. S. Choi, J. Y. Kim, S. H. Lee, K. E. Lee, Y. H. Kim, M. H. Song, S. Yoo and S. O. Kim, *Acs Nano*, 2012, **6**, 159-167.
142. Z. Luo, S. Lim, Z. Tian, J. Shang, L. Lai, B. MacDonald, C. Fu, Z. Shen, T. Yu and J. Lin, *J Mater Chem*, 2011, **21**, 8038-8044.
143. Y. Liu, Q. Feng, N. J. Tang, X. G. Wan, F. C. Liu, L. Y. Lv and Y. W. Du, *Carbon*, 2013, **60**, 549-551.
144. Y. Li, Z. Zhou, P. Shen and Z. Chen, *ACS Nano*, 2009, **3**, 1952-1958.
145. J. W. Chiou, S. C. Ray, S. I. Peng, C. H. Chuang, B. Y. Wang, H. M. Tsai, C. W. Pao, H. J. Lin, Y. C. Shao, Y. F. Wang, S. C. Chen, W. F. Pong, Y. C. Yeh, C. W. Chen, L. C. Chen, K. H. Chen, M. H. Tsai, A. Kumar, A. Ganguly, P. Papakonstantinou, H. Yamane, N. Kosugi, T. Regier, L. Liu and T. K. Sham, *The Journal of Physical Chemistry C*, 2012, **116**, 16251-16258.
146. T. Van Khai, H. G. Na, D. S. Kwak, Y. J. Kwon, H. Ham, K. B. Shim and H. W. Kim, *J Mater Chem*, 2012, **22**, 17992-18003.
147. M. Li, Z. Wu, W. Ren, H. Cheng, N. Tang, W. Wu, W. Zhong and Y. Du, *Carbon*, 2012, **50**, 5286-5291.
148. H.-m. Wang, H.-x. Wang, Y. Chen, Y.-j. Liu, J.-x. Zhao, Q.-h. Cai and X.-z. Wang, *Applied Surface Science*, 2013, **273**, 302-309.
149. Z.-W. Liu, F. Peng, H.-J. Wang, H. Yu, W.-X. Zheng and J. Yang, *Angewandte Chemie International Edition*, 2011, **50**, 3257-3261.
150. T. Schiros, D. Nordlund, L. Palova, D. Prezzi, L. Y. Zhao, K. S. Kim, U. Wurstbauer, C. Gutierrez, D.

Delongchamp, C. Jaye, D. Fischer, H. Ogasawara, L. G. M. Pettersson, D. R. Reichman, P. Kim, M. S. Hybertsen and A. N. Pasupathy, *Nano Letters*, 2012, **12**, 4025-4031.

151. S. Some, J. Kim, K. Lee, A. Kulkarni, Y. Yoon, S. Lee, T. Kim and H. Lee, *Advanced materials*, 2012, **24**, 5481-5486.
152. P. A. Denis, *Computational Materials Science*, 2013, **67**, 203-206.
153. J. Y. Dai and J. M. Yuan, *Journal of Physics-Condensed Matter*, 2010, **22**.
154. K. A. Mkhoyan, A. W. Contryman, J. Silcox, D. A. Stewart, G. Eda, C. Mattevi, S. Miller and M. Chhowalla, *Nano Lett*, 2009, **9**, 1058-1063.
155. D. W. Boukhvalov and M. I. Katsnelson, *Journal of the American Chemical Society*, 2008, **130**, 10697-10701.
156. T. Szabo, O. Berkesi, P. Forgo, K. Josepovits, Y. Sanakis, D. Petridis and I. Dekany, *Chem Mater*, 2006, **18**, 2740-2749.
157. I. Jung, D. A. Dikin, R. D. Piner and R. S. Ruoff, *Nano Lett*, 2008, **8**, 4283-4287.
158. Z. Xu, Y. Bando, L. Liu, W. L. Wang, X. D. Bai and D. Golberg, *Acs Nano*, 2011, **5**, 4401-4406.
159. S. Kim, S. Zhou, Y. K. Hu, M. Acik, Y. J. Chabal, C. Berger, W. de Heer, A. Bongiorno and E. Riedo, *Nat Mater*, 2012, **11**, 544-549.
160. P. V. Kumar, M. Bernardi and J. C. Grossman, *Acs Nano*, 2013, **7**, 1638-1645.
161. H. P. Jia, D. R. Dreyer and C. W. Bielawski, *Tetrahedron*, 2011, **67**, 4431-4434.
162. D. S. Su, J. Zhang, B. Frank, A. Thomas, X. C. Wang, J. Paraknowitsch and R. Schlogl, *Chemsuschem*, 2010, **3**, 169-180.
163. D. R. Dreyer, H. P. Jia and C. W. Bielawski, *Angew Chem Int Edit*, 2010, **49**, 6813-6816.
164. D. R. Dreyer, S. Park, C. W. Bielawski and R. S. Ruoff, *Chemical Society Reviews*, 2010, **39**, 228-240.
165. C. L. Su and K. P. Loh, *Accounts of Chemical Research*, 2013, **46**, 2275-2285.
166. P. A. Denis, *Chemical Physics Letters*, 2010, **492**, 251-257.
167. P. A. Denis, R. Faccio and A. W. Mombru, *Chemphyschem*, 2009, **10**, 715-722.
168. S. Glenis, A. J. Nelson and M. M. Labes, *Journal of Applied Physics*, 1999, **86**, 4464-4466.
169. R. Zboril, F. Karlicky, A. B. Bourlinos, T. A. Steriotis, A. K. Stubos, V. Georgakilas, K. Safarova, D. Jancik, C. Trapalis and M. Otyepka, *Small*, 2010, **6**, 2885-2891.
170. M. A. Ribas, A. K. Singh, P. B. Sorokin and B. I. Yakobson, *Nano Research*, 2011, **4**, 143-152.
171. J. T. Robinson, J. S. Burgess, C. E. Junkermeier, S. C. Badescu, T. L. Reinecke, F. K. Perkins, M. K. Zalalutdniov, J. W. Baldwin, J. C. Culbertson, P. E. Sheehan and E. S. Snow, *Nano Letters*, 2010, **10**, 3001-3005.
172. R. R. Nair, W. C. Ren, R. Jalil, I. Riaz, V. G. Kravets, L. Britnell, P. Blake, F. Schedin, A. S. Mayorov, S. J. Yuan, M. I. Katsnelson, H. M. Cheng, W. Strupinski, L. G. Bulusheva, A. V. Okotrub, I. V. Grigorieva, A. N. Grigorenko, K. S. Novoselov and A. K. Geim, *Small*, 2010, **6**, 2877-2884.
173. K. J. Jeon, Z. Lee, E. Pollak, L. Moreschini, A. Bostwick, C. M. Park, R. Mendelsberg, V. Radmilovic, R. Kostecki, T. J. Richardson and E. Rotenberg, *Acs Nano*, 2011, **5**, 1042-1046.
174. P. V. C. Medeiros, A. J. S. Mascarenhas, F. D. Mota and C. M. C. de Castilho, *Nanotechnology*, 2010, **21**.
175. M. Klintenberg, S. Lebegue, M. I. Katsnelson and O. Eriksson, *Physical Review B*, 2010, **81**.
176. H. Sahin and S. Ciraci, *Journal of Physical Chemistry C*, 2012, **116**, 24075-24083.
177. A. Yaya, C. P. Ewels, I. Suarez-Martinez, P. Wagner, S. Lefrant, A. Okotrub, L. Bulusheva and P. R. Briddon, *Physical Review B*, 2011, **83**.

178. R. Balog, B. Jorgensen, L. Nilsson, M. Andersen, E. Rienks, M. Bianchi, M. Fanetti, E. Laegsgaard, A. Baraldi, S. Lizzit, Z. Sljivancanin, F. Besenbacher, B. Hammer, T. G. Pedersen, P. Hofmann and L. Hornekaer, *Nature Materials*, 2010, **9**, 315-319.
179. D. C. Elias, R. R. Nair, T. M. G. Mohiuddin, S. V. Morozov, P. Blake, M. P. Halsall, A. C. Ferrari, D. W. Boukhvalov, M. I. Katsnelson, A. K. Geim and K. S. Novoselov, *Science*, 2009, **323**, 610-613.
180. M. Pumera and C. H. A. Wong, *Chemical Society Reviews*, 2013, **42**, 5987-5995.
181. S. C. Ray, N. Soin, T. Makgato, C. H. Chuang, W. F. Pong, S. S. Roy, S. K. Ghosh, A. M. Strydom and J. A. McLaughlin, *Scientific Reports*, 2014, **4**.
182. R. Jayasingha, A. Sherehiy, S. Y. Wu and G. U. Sumanasekera, *Nano Letters*, 2013, **13**, 5098-5105.
183. Y. Lee, S. Lee, Y. Hwang and Y. C. Chung, *Applied Surface Science*, 2014, **289**, 445-449.
184. J. Y. Dai, J. M. Yuan and P. Giannozzi, *Applied Physics Letters*, 2009, **95**.
185. Z. M. Ao, J. Yang, S. Li and Q. Jiang, *Chemical Physics Letters*, 2008, **461**, 276-279.
186. J. X. Zhao, Y. Chen and H. G. Fu, *Theoretical Chemistry Accounts*, 2012, **131**.
187. Y. Chen, X. C. Yang, Y. J. Liu, J. X. Zhao, Q. H. Cai and X. Z. Wang, *Journal of Molecular Graphics & Modelling*, 2013, **39**, 126-132.
188. Y. Chen, Y. J. Liu, H. X. Wang, J. X. Zhao, Q. H. Cai, X. Z. Wang and Y. H. Ding, *Acs Applied Materials & Interfaces*, 2013, **5**, 5994-6000.
189. Y. Chen, B. Gao, J. X. Zhao, Q. H. Cai and H. G. Fu, *Journal of Molecular Modeling*, 2012, **18**, 2043-2054.
190. Y. Zou, F. Li, Z. H. Zhu, M. W. Zhao, X. G. Xu and X. Y. Su, *European Physical Journal B*, 2011, **81**, 475-479.
191. H. Nozaki and S. Itoh, *Journal of Physics and Chemistry of Solids*, 1996, **57**, 41-49.
192. B. Sumanta and S. Biplab, 2012.
193. P. Rani and V. K. Jindal, *Appl Nanosci*, 2013, 1-8.
194. B. Muchharla, A. Pathak, Z. Liu, L. Song, T. Jayasekera, S. Kar, R. Vajtai, L. Balicas, P. M. Ajayan, S. Talapatra and N. Ali, *Nano letters*, 2013, **13**, 3476-3481.
195. H. Tachikawa, T. Iyama and K. Azumi, *Japanese Journal of Applied Physics*, 2011, **50**.
196. M. O. Watanabe, S. Itoh, K. Mizushima and T. Sasaki, *Journal of Applied Physics*, 1995, **78**, 2880-2882.
197. M. O. Watanabe, S. Itoh, T. Sasaki and K. Mizushima, *Physical Review Letters*, 1996, **77**, 187-189.
198. B. Muchharla, A. Pathak, Z. Liu, L. Song, T. Jayasekera, S. Kar, R. Vajtai, L. Balicas, P. M. Ajayan, S. Talapatra and N. Ali, *Nano Letters*, 2013, **13**, 3476-3481.
199. X. F. Fan, Z. X. Shen, A. Q. Liu and J. L. Kuo, *Nanoscale*, 2012, **4**, 2157-2165.
200. X. H. Deng, Y. Q. Wu, J. Y. Dai, D. D. Kang and D. Y. Zhang, *Physics Letters A*, 2011, **375**, 3890-3894.
201. C. H. Choi, M. W. Chung, H. C. Kwon, S. H. Park and S. I. Woo, *Journal of Materials Chemistry A*, 2013, **1**, 3694-3699.
202. T. Kwon, H. Nishihara, H. Itoi, Q. H. Yang and T. Kyotani, *Langmuir*, 2009, **25**, 11961-11968.
203. B. Xu, S. F. Yue, Z. Y. Sui, X. T. Zhang, S. S. Hou, G. P. Cao and Y. S. Yang, *Energy & Environmental Science*, 2011, **4**, 2826-2830.
204. V. H. Pham, S. H. Hur, E. J. Kim, B. S. Kim and J. S. Chung, *Chemical Communications*, 2013, **49**, 6665-6667.

205. L. Sun, L. Wang, C. Tian, T. Tan, Y. Xie, K. Shi, M. Li and H. Fu, *RSC Advances*, 2012, **2**, 4498-4506.
206. W. Fan, Y.-Y. Xia, W. W. Tjiu, P. K. Pallathadka, C. He and T. Liu, *Journal of Power Sources*, 2013, **243**, 973-981.
207. P. Karthika, N. Rajalakshmi and K. S. Dhathathreyan, *Journal of Nanoscience and Nanotechnology*, 2013, **13**, 1746-1751.
208. G. Hasegawa, M. Aoki, K. Kanamori, K. Nakanishi, T. Hanada and K. Tadanaga, *Journal of Materials Chemistry*, 2011, **21**, 2060-2063.
209. X. C. Zhao, Q. Zhang, C. M. Chen, B. S. Zhang, S. Reiche, A. Q. Wang, T. Zhang, R. Schlogl and D. S. Su, *Nano Energy*, 2012, **1**, 624-630.
210. H. B. Wang, T. Maiyalagan and X. Wang, *ACS Catal.*, 2012, **2**, 781-794.
211. S. Yang, X. Song, P. Zhang and L. Gao, *ACS Applied Materials & Interfaces*, 2013, **5**, 3317-3322.
212. Y. Y. Liu, V. I. Artyukhov, M. J. Liu, A. R. Harutyunyan and B. I. Yakobson, *Journal of Physical Chemistry Letters*, 2013, **4**, 1737-1742.
213. D. Das, S. Kim, K. R. Lee and A. K. Singh, *Physical Chemistry Chemical Physics*, 2013, **15**, 15128-15134.
214. D. Y. Pan, S. Wang, B. Zhao, M. H. Wu, H. J. Zhang, Y. Wang and Z. Jiao, *Chemistry of Materials*, 2009, **21**, 3136-3142.
215. F. Yao, F. Gunes, H. Q. Ta, S. M. Lee, S. J. Chae, K. Y. Sheem, C. S. Cojocaru, S. S. Xie and Y. H. Lee, *Journal of the American Chemical Society*, 2012, **134**, 8646-8654.
216. C. Ma, X. Shao and D. Cao, *J Mater Chem*, 2012, **22**, 8911-8915.
217. D. H. Wu, Y. F. Li and Z. Zhou, *Theoretical Chemistry Accounts*, 2011, **130**, 209-213.
218. X. L. Wang, Z. Zeng, H. Ahn and G. X. Wang, *Applied Physics Letters*, 2009, **95**.
219. S. H. Gao, Z. Y. Ren, L. J. Wan, J. M. Zheng, P. Guo and Y. X. Zhou, *Applied Surface Science*, 2011, **257**, 7443-7446.
220. Y. X. Yu, *Physical Chemistry Chemical Physics*, 2013, **15**, 16819-16827.
221. X. K. Kong and Q. W. Chen, *Physical Chemistry Chemical Physics*, 2013, **15**, 12982-12987.
222. S. W. Lee, N. Yabuuchi, B. M. Gallant, S. Chen, B. S. Kim, P. T. Hammond and Y. Shao-Horn, *Nat Nanotechnol*, 2010, **5**, 531-537.
223. S. W. Lee, B. S. Kim, S. Chen, Y. Shao-Horn and P. T. Hammond, *Journal of the American Chemical Society*, 2009, **131**, 671-679.
224. C. Z. Zhang, N. Mahmood, H. Yin, F. Liu and Y. L. Hou, *Advanced materials*, 2013, **25**, 4932-4937.
225. Z. L. Wang, D. Xu, H. G. Wang, Z. Wu and X. B. Zhang, *Acs Nano*, 2013, **7**, 2422-2430.
226. X. Wang, X. Q. Cao, L. Bourgeois, H. Guan, S. M. Chen, Y. T. Zhong, D. M. Tang, H. Q. Li, T. Y. Zhai, L. Li, Y. Bando and D. Golberg, *Advanced Functional Materials*, 2012, **22**, 2682-2690.
227. K. Zhang, P. Han, L. Gu, L. Zhang, Z. Liu, Q. Kong, C. Zhang, S. Dong, Z. Zhang, J. Yao, H. Xu, G. Cui and L. Chen, *ACS Applied Materials & Interfaces*, 2012, **4**, 658-664.
228. D. Li, D. Q. Shi, Z. W. Liu, H. K. Liu and Z. P. Guo, *Journal of Nanoparticle Research*, 2013, **15**.
229. F. Zou, X. L. Hu, Y. M. Sun, W. Luo, F. F. Xia, L. Qie, Y. Jiang and Y. H. Huang, *Chemistry-a European Journal*, 2013, **19**, 6027-6033.
230. X. Wang, W. Tian, D. Liu, C. Zhi, Y. Bando and D. Golberg, *Nano Energy*, 2013, **2**, 257-267.
231. D. A. C. Brownson, L. J. Munro, D. K. Kampouris and C. E. Banks, *Rsc Advances*, 2011, **1**, 978-988.

232. Z. H. Sheng, H. L. Gao, W. J. Bao, F. B. Wang and X. H. Xia, *Journal of Materials Chemistry*, 2012, **22**, 390-395.
233. X. G. Bao, X. W. Nie, D. von Deak, E. Biddinger, W. J. Luo, A. Asthagiri, U. Ozkan and C. Hadad, *Topics in Catalysis*, 2013, **56**, 1623-1633.
234. R. Li, Z. D. Wei, X. L. Gou and W. Xu, *Rsc Advances*, 2013, **3**, 9978-9984.
235. X. F. Fan, W. T. Zheng and J. L. Kuo, *Rsc Advances*, 2013, **3**, 5498-5505.
236. Y. Zheng, Y. Jiao, L. Ge, M. Jaroniec and S. Z. Qiao, *Angewandte Chemie-International Edition*, 2013, **52**, 3110-3116.
237. X. K. Kong, Q. W. Chen and Z. Y. Sun, *Chemphyschem*, 2013, **14**, 514-519.
238. L. P. Zhang and Z. H. Xia, *Journal of Physical Chemistry C*, 2011, **115**, 11170-11176.
239. Z. P. Jin, H. G. Nie, Z. Yang, J. Zhang, Z. Liu, X. J. Xu and S. M. Huang, *Nanoscale*, 2012, **4**, 6455-6460.
240. A. G. Garcia, S. E. Baltazar, A. H. R. Castro, J. F. P. Robles and A. Rubio, *Journal of Computational and Theoretical Nanoscience*, 2008, **5**, 2221-2229.
241. C. Z. Zhu and S. J. Dong, *Nanoscale*, 2013, **5**, 1753-1767.
242. Z. Yang, H. G. Nie, X. Chen, X. H. Chen and S. M. Huang, *Journal of Power Sources*, 2013, **236**, 238-249.
243. Y. Y. Liang, Y. G. Li, H. L. Wang, J. G. Zhou, J. Wang, T. Regier and H. J. Dai, *Nature Materials*, 2011, **10**, 780-786.
244. Z. Q. Luo, S. H. Lim, Z. Q. Tian, J. Z. Shang, L. F. Lai, B. MacDonald, C. Fu, Z. X. Shen, T. Yu and J. Y. Lin, *Journal of Materials Chemistry*, 2011, **21**, 8038-8044.
245. H. Kim, K. Lee, S. I. Woo and Y. Jung, *Physical Chemistry Chemical Physics*, 2011, **13**, 17505-17510.
246. K. R. Lee, K. U. Lee, J. W. Lee, B. T. Ahn and S. I. Woo, *Electrochemistry Communications*, 2010, **12**, 1052-1055.
247. H. R. Byon, J. Suntivich and Y. Shao-Horn, *Chemistry of Materials*, 2011, **23**, 3421-3428.
248. K. Kamiya, K. Hashimoto and S. Nakanishi, *Chemical Communications*, 2012, **48**, 10213-10215.
249. X. Q. Xie, J. L. Long, J. Xu, L. M. Chen, Y. Wang, Z. Z. Zhang and X. X. Wang, *Rsc Advances*, 2012, **2**, 12438-12446.
250. R. T. Lv, T. X. Cui, M. S. Jun, Q. Zhang, A. Y. Cao, D. S. Su, Z. J. Zhang, S. H. Yoon, J. Miyawaki, I. Mochida and F. Y. Kang, *Advanced Functional Materials*, 2011, **21**, 999-1006.
251. H. Z. Dong, J. C. Bai, Q. Q. Zhu, J. H. Yu, L. Y. Yu and L. F. Dong, *Journal of Renewable and Sustainable Energy*, 2013, **5**.
252. J. D. Roy-Mayhew, D. J. Bozym, C. Punckt and I. A. Aksay, *Acs Nano*, 2010, **4**, 6203-6211.
253. X. B. Xu, D. K. Huang, K. Cao, M. K. Wang, S. M. Zakeeruddin and M. Gratzel, *Scientific Reports*, 2013, **3**.
254. Y. H. Xue, J. Liu, H. Chen, R. G. Wang, D. Q. Li, J. Qu and L. M. Dai, *Angewandte Chemie-International Edition*, 2012, **51**, 12124-12127.
255. X. Y. Zhang, S. P. Pang, X. Chen, K. J. Zhang, Z. H. Liu, X. H. Zhou and G. L. Cui, *Rsc Advances*, 2013, **3**, 9005-9010.
256. M. J. Ju, J. C. Kim, H.-J. Choi, I. T. Choi, S. G. Kim, K. Lim, J. Ko, J.-J. Lee, I.-Y. Jeon, J.-B. Baek and H. K. Kim, *ACS Nano*, 2013, **7**, 5243-5250.
257. S. Das, P. Sudhagar, V. Verma, D. Song, E. Ito, S. Y. Lee, Y. S. Kang and W. Choi, *Advanced*

Functional Materials, 2011, **21**, 3729-3736.

258. X. M. Li, D. Xie, H. Park, M. Zhu, T. H. Zeng, K. L. Wang, J. Q. Wei, D. H. Wu, J. Kong and H. W. Zhu, *Nanoscale*, 2013, **5**, 1945-1948.
259. G. H. Jun, S. H. Jin, B. Lee, B. H. Kim, W.-S. Chae, S. H. Hong and S. Jeon, *Energy & Environmental Science*, 2013, **6**, 3000-3006.
260. Y. Y. Shao, S. Zhang, M. H. Engelhard, G. S. Li, G. C. Shao, Y. Wang, J. Liu, I. A. Aksay and Y. H. Lin, *Journal of Materials Chemistry*, 2010, **20**, 7491-7496.
261. G. H. Yang, Y. H. Zhou, J. J. Wu, J. T. Cao, L. L. Li, H. Y. Liu and J. J. Zhu, *Rsc Advances*, 2013, **3**, 22597-22604.
262. Y. Wang, Y. Y. Shao, D. W. Matson, J. H. Li and Y. H. Lin, *Acs Nano*, 2010, **4**, 1790-1798.
263. Z. H. Sheng, X. Q. Zheng, J. Y. Xu, W. J. Bao, F. B. Wang and X. H. Xia, *Biosens Bioelectron*, 2012, **34**, 125-131.
264. S. M. Li, S. Y. Yang, Y. S. Wang, C. H. Lien, H. W. Tien, S. T. Hsiao, W. H. Liao, H. P. Tsai, C. L. Chang, C. C. M. Ma and C. C. Hu, *Carbon*, 2013, **59**, 418-429.
265. H. X. Fan, Y. Li, D. Wu, H. M. Ma, K. X. Mao, D. W. Fan, B. Du, H. Li and Q. Wei, *Anal Chim Acta*, 2012, **711**, 24-28.
266. P. P. Guo, F. Xiao, Q. Liu, H. F. Liu, Y. L. Guo, J. R. Gong, S. Wang and Y. Q. Liu, *Scientific Reports*, 2013, **3**.
267. Y. X. Huang, X. C. Dong, Y. X. Liu, L. J. Li and P. Chen, *Journal of Materials Chemistry*, 2011, **21**, 12358-12362.
268. Y. Q. Wen, F. B. Y. Li, X. C. Dong, J. Zhang, Q. H. Xiong and P. Chen, *Advanced Healthcare Materials*, 2013, **2**, 271-274.
269. Y. H. Zhang, Y. B. Chen, K. G. Zhou, C. H. Liu, J. Zeng, H. L. Zhang and Y. Peng, *Nanotechnology*, 2009, **20**.
270. Y. H. Zhang, L. F. Han, Y. H. Xiao, D. Z. Jia, Z. H. Guo and F. Li, *Computational Materials Science*, 2013, **69**, 222-228.
271. J. Y. Dai and J. M. Yuan, *Physical Review B*, 2010, **81**.
272. F. Niu, J. M. Liu, L. M. Tao, W. Wang and W. G. Song, *Journal of Materials Chemistry A*, 2013, **1**, 6130-6133.
273. H. Xu, L. M. Xie, H. L. Zhang and J. Zhang, *Acs Nano*, 2011, **5**, 5338-5344.
274. X. K. Kong and Q. W. Chen, *J Mater Chem*, 2012, **22**, 15336-15341.
275. R. Lv, Q. Li, A. R. Botello-Mendez, T. Hayashi, B. Wang, A. Berkdemir, Q. Z. Hao, A. L. Elias, R. Cruz-Silva, H. R. Gutierrez, Y. A. Kim, H. Muramatsu, J. Zhu, M. Endo, H. Terrones, J. C. Charlier, M. H. Pan and M. Terrones, *Sci Rep-Uk*, 2012, **2**.
276. V. Tozzini and V. Pellegrini, *Physical Chemistry Chemical Physics*, 2013, **15**, 80-89.
277. V. B. Parambhath, R. Nagar and S. Ramaprabhu, *Langmuir*, 2012, **28**, 7826-7833.
278. S. Lee, M. Lee, H. Choi, D. S. Yoo and Y. C. Chung, *International Journal of Hydrogen Energy*, 2013, **38**, 4611-4617.
279. S. Lee, M. Lee and Y. C. Chung, *Physical Chemistry Chemical Physics*, 2013, **15**, 3243-3248.
280. Y. G. Zhou, X. T. Zu, F. Gao, J. L. Nie and H. Y. Xiao, *Journal of Applied Physics*, 2009, **105**, 014309-014309-014304.
281. E. Beheshti, A. Nojeh and P. Servati, *Carbon*, 2011, **49**, 1561-1567.
282. K. C. Kemp, V. Chandra, M. Saleh and K. S. Kim, *Nanotechnology*, 2013, **24**.
283. W. L. Wei, C. Xu, L. Wu, J. S. Wang, J. S. Ren and X. G. Qu, *Scientific Reports*, 2014, **4**.

284. Q. Liu, B. D. Guo, Z. Y. Rao, B. H. Zhang and J. R. Gong, *Nano Letters*, 2013, **13**, 2436-2441.
285. D. Sun, R. Ban, P. H. Zhang, G. H. Wu, J. R. Zhang and J. J. Zhu, *Carbon*, 2013, **64**, 424-434.
286. A. D. Zhao, C. Q. Zhao, M. Li, J. S. Ren and X. G. Qu, *Analytica Chimica Acta*, 2014, **809**, 128-133.